PERFORMANCE ANALYSIS OF A HELIUM COOLED VHTR POWERED BRAYTON CYCLE TOPPING UNIT ON AN EXISTING STEAM CYCLE USING NUMERICAL PROPULSION SYSTEM SIMULATION

by

WARREN ROMAO CAETANO FREITAS

Presented to the Faculty of the Graduate School of
The University of Texas at Arlington in Partial Fulfillment
of the Requirements
for the Degree of

MASTER OF SCIENCE IN MECHANICAL ENGINEERING

THE UNIVERSITY OF TEXAS AT ARLINGTON

MAY 2015

Acknowledgements

I would like to thank my thesis adviser Dr. Donald Wilson for his valuable guidance, encouragement and the vast amount of patience he has had with me. I extend my thanks to Dr. Frank Lu, Dr. Brian Dennis and Mr. Bill Simpkin for their ideas and feedback, without which this thesis would not have been possible.

I am thankful to my colleagues Purushotham Balaji, Hatim Rangwala, Vijay Gopal, Nanda Kumar and Umang Dighe for their help and feedback.

I also express my deepest gratitude to my Mom and Dad, Wayne and Rinu. Your support and constant encouragement have been a blessing.

April 13, 2015

Abstract

PERFORMANCE ANALYSIS OF A HELIUM COOLED VHTR POWERED BRAYTON CYCLE TOPPING UNIT ON AN EXISTING STEAM CYCLE USING NUMERICAL PROPULSION SYSTEM SIMULATION

Warren Romao Caetano Freitas, M.S.

The University of Texas at Arlington, 2015

Supervising Professor: Donald R. Wilson

With the decommissioning of ageing coal power plants due to outdated technology and high levels of air pollution, the advantages of overhauling existing infrastructure is twofold. First, by providing an alternate, sustainable fuel source, like nuclear power, the problem of air pollution can be brought to check. Second, utilizing existing steam plant infrastructure reduces initial investment costs and allows investors to keep the existing steam plant running until the new infrastructure is ready to go online.

The focus of this research is to design and analyze the topping cycle required to support an existing 300 MW_e power plant based on the Hi Eff Mod™ patent. The system is designed and simulated using the Numerical Propulsion System Simulation software. The highly robust solver uses a modified Newton-Raphson technique to iteratively find a solution to the set of non-linear equations. The use of compressor and turbine maps provides for quick and accurate analysis of the cycle off-design operation. The Brayton cycle is an indirectly fired gas turbine system that uses helium as the working fluid and a nuclear reactor as its heat source. The Brayton cycle is designed based on the existing steam cycle and both cycles are analyzed for part load performance.

Table of Contents

List of Illustrations

List of Tables

Chapter 1

Introduction

This chapter discusses the motivation and the main idea behind this research. It also provides a brief discussion of the thermodynamic cycles that will be simulated i.e. the Rankine cycle, the Brayton cycle and the combined cycle that encompasses the Brayton cycle as the topping cycle and the Rankine cycle as the bottoming cycle. A brief discussion is also provided on the Pebble Bed Modular Reactor (PBMR), the GTHTR300 turbomachinery used in the Brayton cycle and the Hi Eff Mod™ patent.

1.1 Motivation

Coal-fired power plants generate more than 50 percent of the electricity in the United States and produce about 40 percent of the country's CO_2 emissions [1]. Due to high and unacceptable levels of atmospheric pollution, various techniques are being developed to reduce CO_2 emissions. One method is to capture and store the CO_2 [2] while another attempts to filter the flue gases [3]. A patent by William Edward Simpkin consists of a helium gas turbine/very high temperature reactor (VHTR) topping unit that could be integrated with an existing steam power plant. By replacing the existing ageing coal-fired boilers with an alternate heat source, clean electricity can be generated [4]. This research simulates the power plant model to determine the topping cycle configuration given an existing steam cycle configuration.

1.2 Cycle Operation

1.2.1 Brayton Cycle

A gas turbine engine works on the principle of the Brayton or Joule cycle. The ideal Brayton cycle consists of four processes:

- Isentropic compression

- Isobaric heat addition
- Isentropic expansion
- Isobaric heat rejection

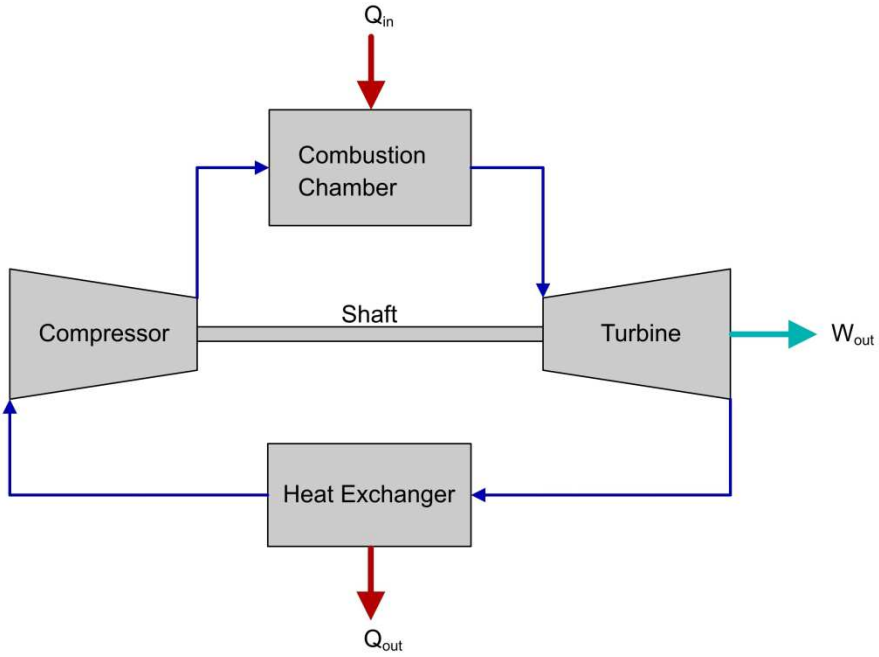

Figure 1-1 Closed loop Brayton cycle

The Brayton cycle can be either an open cycle, as in the case of a jet engine or a closed cycle, as shown in Figure 1-1. Based on the efficiency of the ideal Brayton cycle, we have the upper limit on the efficiency of the real cycle. Figure 1-2 shows the (a) T-s diagram and (b) P-v diagram.

For a real cycle, the compression and expansion processes are not isentropic i.e. they are irreversible. However, they are adiabatic as there is no heat entering or leaving the system. Useful work is dissipated due to the increase in entropy resulting in a lower efficiency [5]. The pressure losses in the combustion chamber and heat exchanger results in the compressor having to perform extra work to maintain the required pressure.

These losses contribute to lower efficiency values. In this cycle, the turbine provides the power to run the compressor. A substantial part of the work produced by the turbine is drawn by the compressor, which in some cases, can reach values as high as 80 percent of turbine shaft work [5]. The remaining power that is generated by the turbine is converted to useful work.

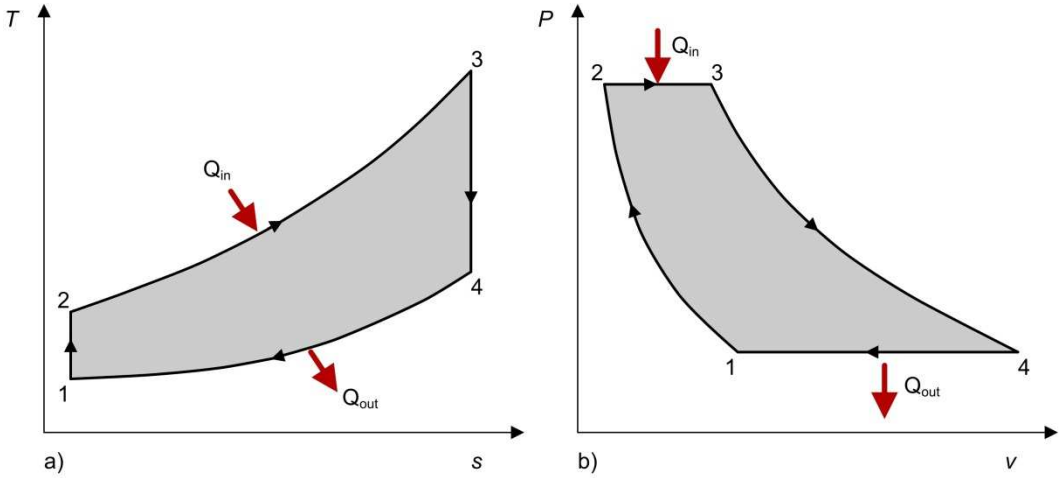

Figure 1-2 Brayton cycle (a) temperature-specific entropy diagram; (b) Pressure-specific volume diagram

1.2.2 Rankine Cycle

Steam power plants work on the principle of the Rankine cycle. The ideal Rankine cycle consists of the following four processes:

- Isentropic compression
- Isobaric heat addition with phase change to a superheated state
- Isentropic expansion
- Isobaric heat rejection with phase change to saturated liquid state

Figure 1-3 shows the ideal Rankine cycle. Based on the efficiency of the ideal cycle, we have the upper limit on the efficiency of the real cycle.

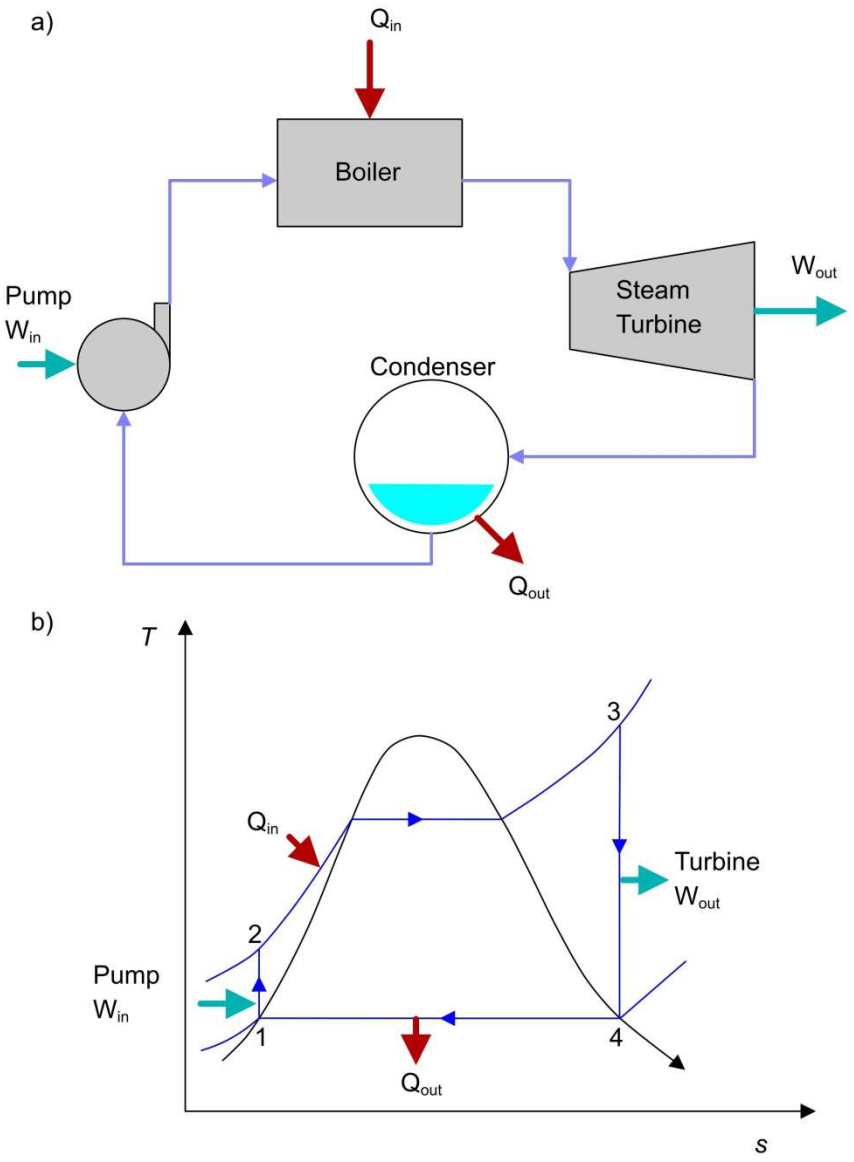

Figure 1-3 (a) Simple Rankine cycle (b) Temperature-specific entropy diagram

Like the real Brayton cycle, the real Rankine cycle has a lower efficiency than its ideal cycle due to irreversibility and pressure losses. The most common fluid used in this cycle is water, but other fluids can also be used [5]. Recent trends have been to use organic fluids instead of water as the working fluid. An organic Rankine cycle (ORC)

generates shaft work from low to medium temperature heat sources with higher thermodynamic efficiency [6]. ORCs can be powered by solar energy or recovered waste heat and are used in small to medium installations [5].

1.2.3 Combined Cycle

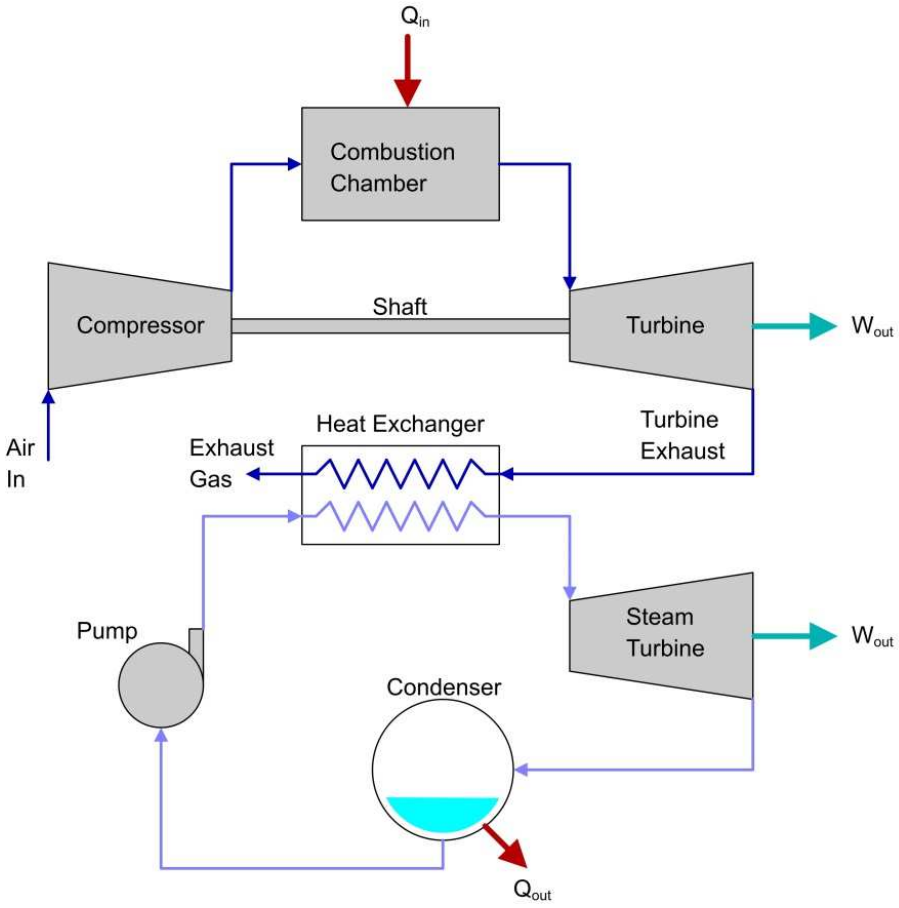

Figure 1-4 Combined Brayton-Rankine cycle

The turbine exhaust in a Brayton cycle is typically at a high temperature allowing further work to be extracted from the flow [5]. Recovering this heat from the exhaust to produce additional work has economic and environmental advantages [5]. In the case of power generation, it can be used to produce steam to power a steam turbine. Since the

heat added to the combined cycle remains constant and there is a net increase in work output, the overall cycle efficiency is improved.

The configuration in Figure 1-4 has one gas turbine for one steam turbine. Other configurations such as one gas turbine and two steam turbines or two gas turbines and three steam turbines are possible depending on the individual turbomachinery design [5]. Coupling of the Brayton and Rankine cycles through a heat recovery steam generator requires more than just the energy conservation analysis [5]. Physical constraints on operating conditions such as pinch temperatures and mass flow rates govern the operation of the heat recovery steam generator [5]. This has an effect on the sizing of the steam turbine [5].

1.3 Pebble Bed Modular Reactor

As described by Schofield [7], modular reactors have an economic and logistical advantage over conventional power generation methods. High Temperature Gas Reactors (HTGR) are configured with either a prismatic core or a pebble bed [7]. The online refueling capability of the pebble bed reactor, i.e. the ability to change the fuel while the reactor is still critical, allows for checks on integrity and consumption of fuel pebbles before being recirculated [7]. Due to the online refueling capability of the pebble bed design, down times are determined by the turbomachinery maintenance schedule which is estimated to have a six year interval [7].

The HTGR core, as explained by Wang [8], is designed to have a high heat capacity and negative temperature coefficient of reactivity; the coolant is inert and is highly stable and the fuel particles have the capability to retain the fission products. He also states that passive cooling techniques effectively prevent the fuel temperature from exceeding the failure temperature, a unique characteristic of the modular type HTGR. These features account for the excellent safety characteristics of the HTGR.

The two options under development are:

• A direct cycle helium gas turbine system being developed by Eskom [9]

• An indirect helium to helium intermediate heat exchanger (IHX) gas turbine system being developed by MIT [9].

In the direct cycle, the high temperature working fluid exits the reactor core and is sent to the turbomachinery where work is extracted before being recirculated to the reactor core [8]. In the indirect cycle, the primary circuit transfers heat via the IHX to a secondary circuit which contains the turbomachinery [9]. The circulator controls the mass flow rate of the working fluid through the primary circuit and provides the required pressure head to overcome the primary circuit pressure losses [8].

The direct cycle has the advantage of fewer components resulting in higher efficiencies [8]. Disadvantages of a direct cycle include higher maintenance and component costs due to the possibility of contamination of the power unit, and in the event of turbine blade failure, damage to the circuit walls could result in leakage of the coolant [8].

In the indirect cycle, the temperature drop between the primary circuit and secondary circuit, due to the IHX, lowers the efficiency of the indirect cycle [8]. Similar to the direct cycle, a depressurization accident occurring in one circuit imposes a high pressure differential on the IHX, and could cause the IHX to fail [8]. However, since the turbomachinery operates on a separate loop, the possibility of contamination in the power conversion unit no longer exists, making maintenance simple and allowing for components to be built to non-nuclear standards [8]. In this study, the pebble bed reactor is used with helium as the working fluid and follows the direct cycle helium turbine system.

1.4 GTHTR300 Turbo-machinery

Takizuka et al. [10] describes the design of the GTHTR300 turbomachinery developed by the Japan Atomic Energy Research Institute. The GTHTR300 operates on the Brayton cycle and utilizes helium as the working fluid [10]. The cycle is nonintercooled, and utilizes a recuperator to increase cycle efficiency [10]. The system consists of a 600 MW_{th} reactor core, a turbo-compressor, an electric generator, a recuperator and a pre-cooler that are connected through coaxial double piping [10].

Figure 1-5 shows the schematic flow diagram of the GTHTR300 primary system. Helium is heated from 824 to 1087 K in the reactor core and enters the turbine at 6.88 MPa [10]. The flow expands through the turbine to 3.68 MPa at 855 K and enters the recuperator where it transfers its heat to the high pressure flow from the compressor and cools to 404 K [10]. The flow then enters the precooler where a cooling water system cools it further to 265 K. This cool helium is then compressed in the compressor to 7.11 MPa, at 374 K [10]. The high pressure helium from the compressor enters the recuperator and absorbs heat from the low pressure helium and is heated to 824 K [10]. The high pressure flow from the recuperator is sent to the reactor core and completes the closed cycle [10].

The GTHTR300 compressor is an axial flow compressor with a pressure ratio of 2.0 [10]. The 20-stage axial-flow compressor has a boss ratio (ratio of hub to tip radius) of about 0.9 and the 20 stages are preceded by inlet guide vanes and followed by outlet guide vanes [10]. The end-wall contours are nearly parallel to the axis of the compressor [10]. The flow passage slowly narrows downstream to improve flow stability [10]. *"A large number of compressor stages relative to the pressure ratio, high boss ratio, and a nearly parallel flow passage are salient features unique to the helium gas compressor. This stems from a larger specific heat of helium gas than that of air"* [10].

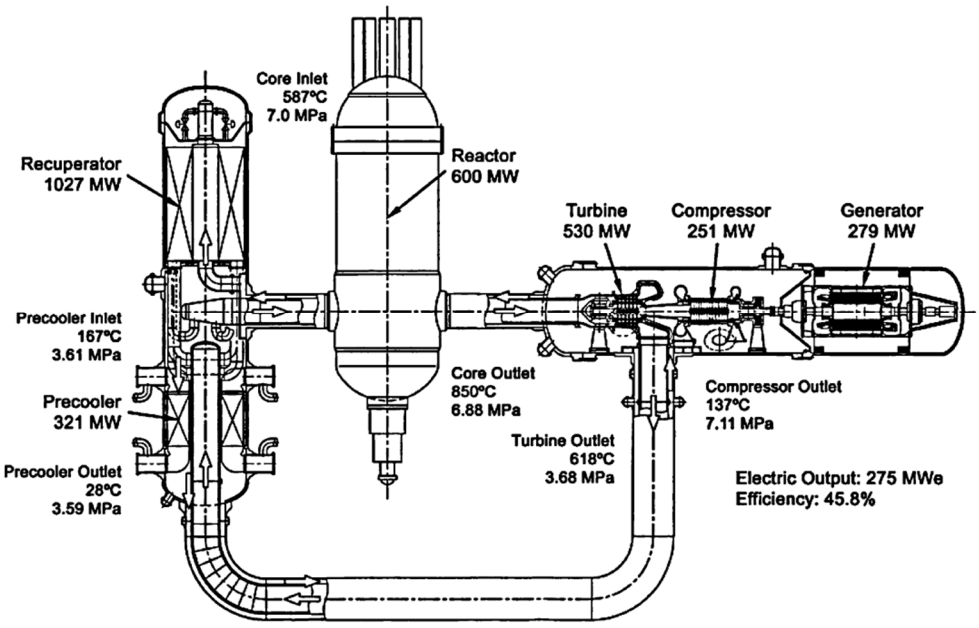

Figure 1-5 Schematic flow diagram of the GTHTR300 primary system [10]

A smooth flow field with no flow separation around the rotor or stator blades was confirmed by three dimensional viscous flow simulation [10]. The GTHTR300 compressor was predicted to have a design point polytropic efficiency of 90.5 percent with a 30 percent surge margin [10].

The six-stage axial flow helium turbine was designed to have a pressure ratio of 1.87, a predicted polytropic efficiency of 92.8 percent and a low turbine bypass flow of around 1 percent at design point [10]. It has a boss ratio of 0.855 at the first stage and 0.778 at the last stage [10]. For the same reasons as the compressor, the turbine too has a higher boss ratio and a greater number of stages than a combustion gas turbine [10]. Leakage losses are reduced by providing rotor blades with finned shrouds at the blade tip, and to reduce secondary and profile losses, the stator blades are bowed [10].

The electric generator operates at an efficiency of 98.5 percent and converts 297 MW shaft power to 275 MW_e electric output [10]. Fig1-7 shows the longitudinal cross-section of the GTHTR300 turbo-machine.

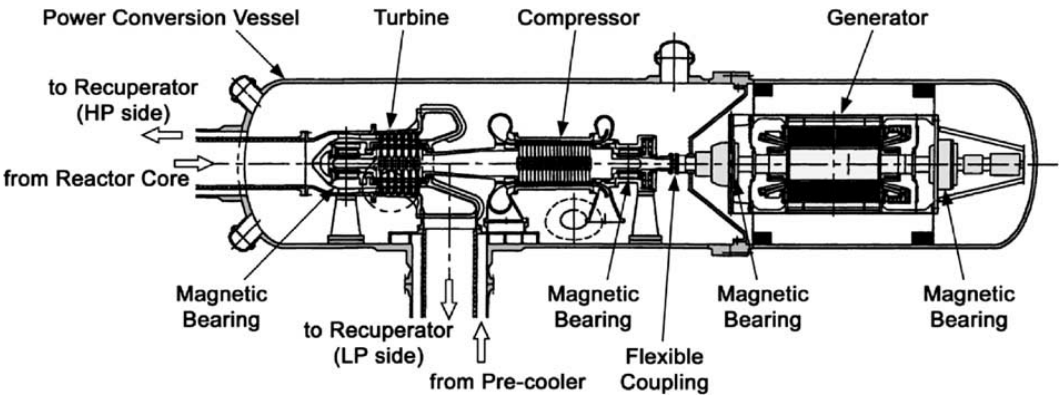

Figure 1-6 Longitudinal cross-section of the GTHTR300 turbo-machine[10]

A report by Sandia National Labs addresses the off-design performance of the GTHTR300 turbomachinery [11]. It predicts the variation of polytropic efficiencies, pressure ratios, exit temperatures and pressure losses, among others, of the turbine and compressor at different rpm values [11]. The graphs of the predicted polytropic efficiency of the GTHTR300 turbine and compressor are shown in Figure 1-7 and Figure 1-8.

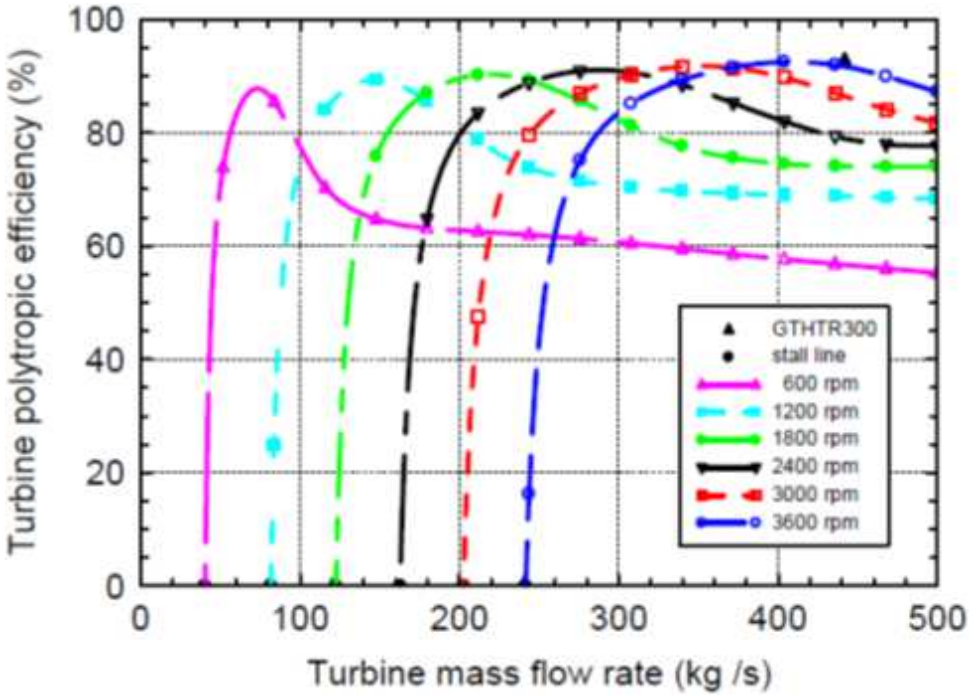

Figure 1-7 Predicted polytropic efficiency of GTHTR300 turbine [11]

At constant shaft speed, inlet temperature, and pressure, the turbine work output and pressure ratio decrease with decreasing mass flow rate [11]. The polytropic efficiency starts dropping very quickly as mass flow rate reduces (as the pressure ratio drops towards 1), eventually reaching zero when the turbine work to the shaft vanishes [11]. It is also found that pressure losses cause the turbine to stall at a pressure ratio slightly greater than 1 [11].

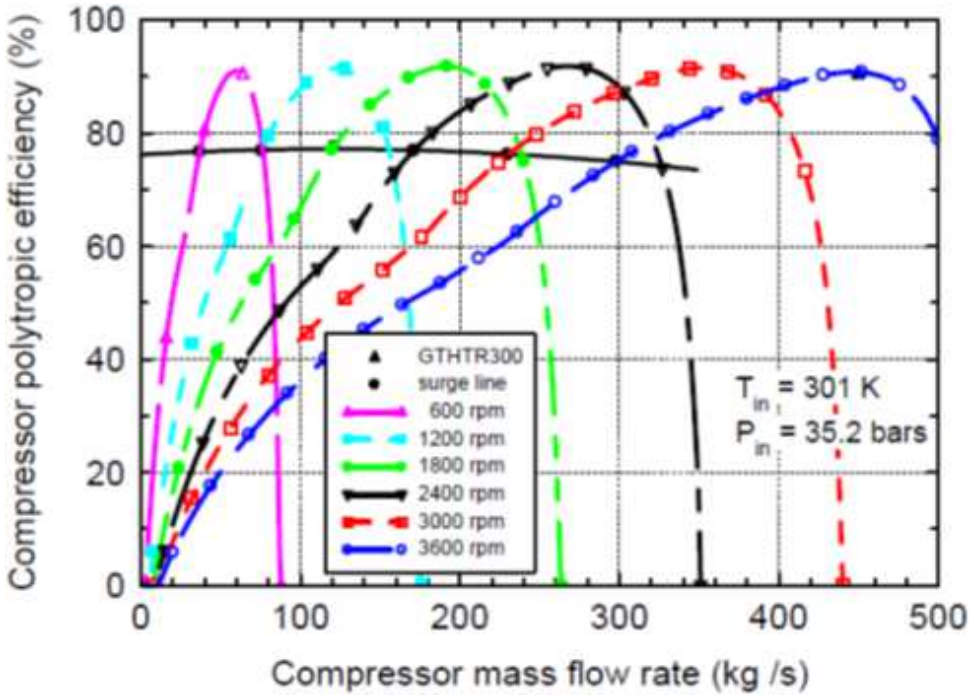

Figure 1-8 Predicted polytropic efficiency of GTHTR300 compressor [11]

As for the compressor, when the mass flow rate of helium is reduced below its design point, the compressor blade experiences an increase in the angle of attack resulting in a rapid increase in pressure losses [11]. The compressor polytropic efficiency also decreases steadily from its peak value as seen in Figure 1-9 [11]. In this study, the trends in variation of polytropic efficiency with mass flow rate are used to simulate the off-design performance of the helium turbomachinery.

1.5 Hi Eff Mod™ Patent

"The High Efficiency ("Hi Eff Mod") Utility Rescue® is a patented power generation system designed to replace the coal-fired boilers of existing worn out fossil-fueled plants as well as Generation III depleted nuclear power plants slated for retirement" [12].

The patent [4] proposes the use of the U.S. DOE Generation IV Helium-cooled VHTR as the heat source and a helium compressor and electric generator that are coupled to a helium turbine. High pressure helium, which acts as a coolant, is pumped into the reactor by the compressor [4]. The high temperature helium exiting the reactor core drives the helium turbine to produce electricity [4]. A heat exchanger is connected to the exit of the turbine and transfers heat from the turbine exhaust to an existing steam boiler [4]. By utilizing exhaust heat from the Brayton cycle, the need to burn fuel to produce steam can be reduced or eliminated completely [12].

The cycle is a closed loop Brayton cycle with the main feature of this system being a helium reservoir tank [4]. The tank is connected to the outlet of the compressor via a control valve [4]. The tank provides the capability of controlling the mass flow rate of helium through the system, thus varying the power generated by the Brayton cycle [4].

Chapter 2

Numerical Propulsion System Simulation

This chapter begins by providing an overview of Numerical Propulsion System Simulation (NPSS). This is followed by a discussion of the Fluid Property Table (FPT) feature of NPSS and the development of the NPSS setup.

2.1 Overview

NPSS is a joint effort between NASA and other Government agencies, industry, and universities to integrate propulsion technologies with high-performance computing and communications technologies into a complete system for performing detailed full-engine simulations [13]. NPSS' architecture is developed based on the object-oriented paradigm [14]. The tool was written with the assumption that most users would desire to easily add their own unique objects and calculations without the burden of modifying the source code [13].

"NPSS is capable of performing multi-disciplinary simulations by combining the main stream propulsion calculations along with aerodynamics, fluid dynamics, structures and heat transfer" [15]. According to Follen [16], a key feature of NPSS is the ability to link tools at various levels of analysis detail, or multi-fidelity, thus allowing the user to transition from 0-dimensional engine cycle analyses to 1-dimensional mean line design tools and 3-dimensional CFD tools. This feature, named "zooming", provides several advantages in design and development of an engine. Engine component designs can be integrated and compared accurately and rapidly as boundary conditions like pressure, temperature, flow, etc. at the inlet and exit of the component as well as results of the entire engine performance are available to the designer [16]. This improves the fidelity of the analysis as the impact of the component on the system is evaluated [16]. By basing

the component analysis on 1st principle analysis codes, the engine simulation can be made more predictive [16]. With the zooming feature, the resolution and fidelity of the engine model can be tailored to match the analysis requirements and high fidelity analysis can be limited to the required components, saving computation time and resources [16].

Mark [17] used NPSS to perform a high fidelity, three-dimensional simulation of the GE90 engine. He simulated the turbine and compressor using APNASA turbomachinery flow code and the combustion chamber was simulated using National Combustor Code. A complete three-dimensional analysis of the turbine engine near cycle conditions was reportedly carried out within 10 hours and 20 minutes. Similar research carried out by Russell, et al. [18] successfully uses NPSS's zooming technique on a turbine engine with three levels of fidelity; zero-dimensional calculations carried out by NPSS, one-dimensional calculations are taken care by mean line analysis codes, namely STGSTK and BRSTK for compression systems and AXOD for turbine components. APNASA provided a detailed, three-dimensional analysis and the communication between the codes was automated using NPSS [18].

2.2 Thermodynamic Property Package

NPSS offers the user the ability to define or select which thermodynamics package to use for calculations involving fluid properties [19]. NPSS comes with a few predefined thermodynamic property packages, namely, allFuel, GasTbl and Janaf, and a provision to accommodate custom fluids through the FPT.

The allFuel thermo package can be used to define the thermodynamic state of a gaseous mixture composed of air, water vapor, and a variety of fuels [19]. GasTbl consists of three property tables (GASTAB, GASEQL, and GASEQL2) and can be used to define the thermodynamic state of a gaseous mixture composed of air, water vapor,

and a JP-class hydrocarbon fuel [19]. The Janaf thermodynamic package is used to calculate the equilibrium solution of mixtures typical for a hydrocarbon fuel combusted in air [19].

As described in the NPSS thermodynamic property package user guide [19], the fluid property table's FlowStation was developed to allow users to model thermodynamic properties for fluids not in the standard NPSS packages. The fluid's thermodynamic properties are defined by the user in an ".fpt" file [19]. The fluid data can be in the form of NPSS tables or functions that return a "real" data type value [19].

2.3 Development of NPSS Code

The first step in NPSS is usually to specify the fluid property package. This lets NPSS calculate the properties of the fluid as it flows through each component. Since the thermodynamic packages in NPSS did not account for helium, one of the first steps was to develop a fluid property table for helium.

The National Institute of Standards and Technology (NIST) provides thermophysical properties of several fluids. By following the syntax given in the NPSS User Guide, the helium FPT was created for pressures varying from 689.47 Pa (absolute) to 10.34 MPa (absolute). The intermediate values are interpolated by the solver using a linear interpolation technique. The range of helium pressure values in the table was carefully selected to account for a large range of pressure and temperature cases.

The helium circuit and components were simulated using the helium fluid property table. The steam cycle was operated using a separate fluid property table with water and steam properties. Both tables were created using NIST's thermophysical properties of fluid systems' webbook [20].

The next step was to define the elements of the cycle. A schematic diagram of the combined cycle plant is shown in Figure 2-1. The turbine and compressor elements

were based on NPSS's existing model. Two shaft elements were created, one to connect the turbine, compressor, and generator in the Brayton cycle and the other to connect the turbine and generator in the steam cycle. The nuclear reactor was modeled as a heat source.

A single heat exchanger was setup to calculate the heat transfer from the Brayton cycle to the steam cycle. In addition to the patent design, a heat sink that functions like a condenser was added in parallel to the heat exchanger. A splitter was added before the heat exchanger to bypass the excess helium flow during part-load operation of the steam cycle. The cool helium from the heat exchanger and the sink are combined and sent to the compressor. With this modification to the heat exchanger setup, only the required amount of helium is sent to the heat exchanger to produce steam and the excess helium is cooled in the sink.

In the steam cycle, apart from the heat exchanger, turbine, shaft and generator elements, the cycle also contains a condenser and a water pump. The condenser acts as the cycle's heat sink and converts the steam to water. The pump is used to recycle the water from the condenser back to the heat exchanger, thus completing the loop. The pump functions independently and by varying the pump rpm, the pressure and mass flow rate of steam can be controlled. The steam turbine and water pump was modeled using the turbine map and pump characteristics from Wolverine Ventures [21]. After initializing the component's variables, the simulation is executed, and NPSS performs iterations till the dependent variables have been satisfied. The "TurbinePRmap" manages the calculation of turbine performance with function calls to map files that return efficiency and corrected weight flow values as a function of corrected speed and pressure ratio [21].

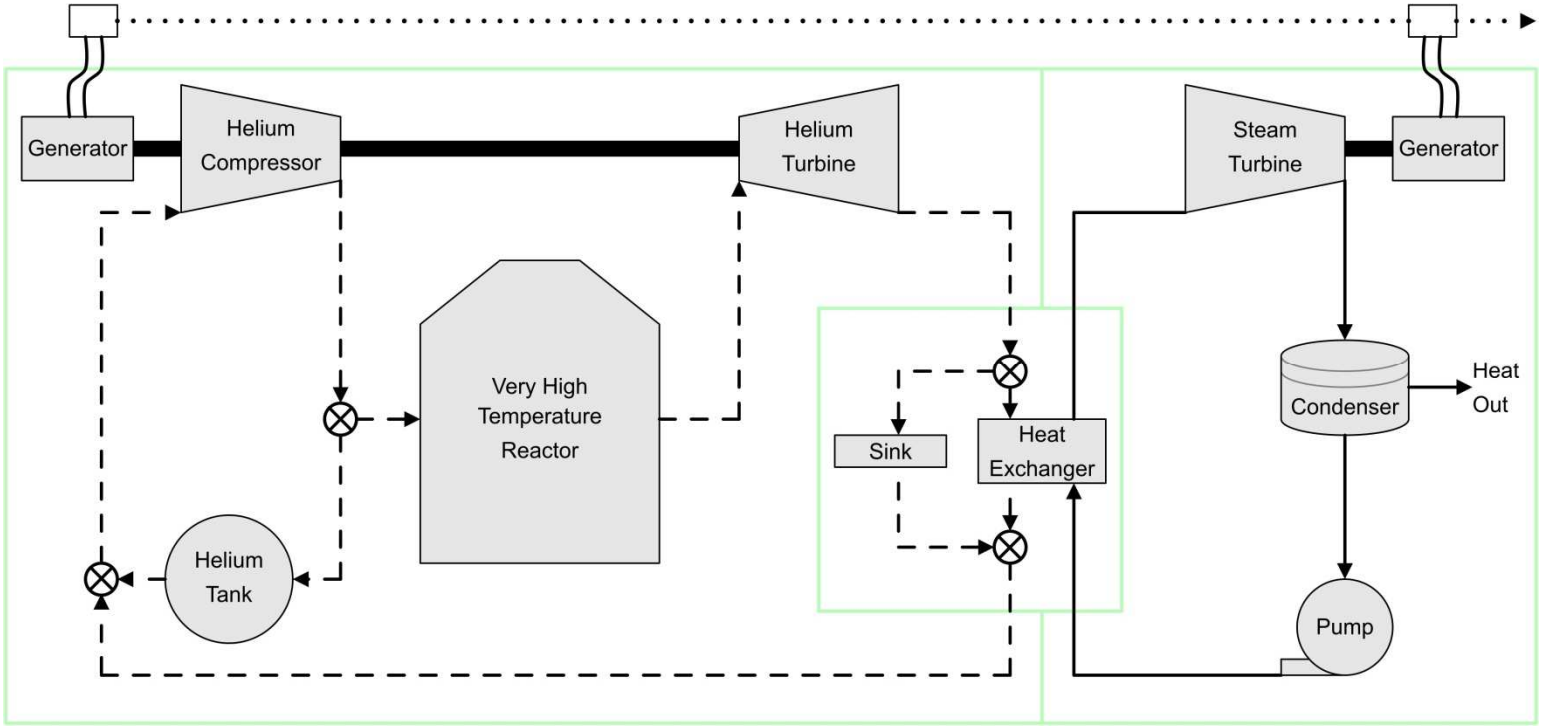

Figure 2-1 Schematic diagram of the combined cycle plant

To simulate the helium compressor and turbine elements at part load, the trends in variation of polytropic efficiency of the GTHTR300 compressor and turbine were used [11]. From the Sandia National Laboratory report [11], the variation in polytropic efficiency with mass flow rate was obtained for both the turbine and the compressor. By calculating the percentage change in polytropic efficiency with percentage change in off-design mass flow rate, the trends in off-design polytropic efficiency variation of the turbine and compressor was obtained. Using these trends, the efficiency values based on a design point polytropic efficiency of 92.8 percent for the turbine and a polytropic efficiency of 90.5 percent for the compressor were stored in tabular form. The trends were calculated for 3600 rpm and up to a mass fraction of 70 percent of design point value. A function was called that returns the polytropic efficiency by reading the table (see Appendix A). NPSS then varies the adiabatic efficiency of the turbine and compressor until it corresponds to the small-stage efficiency value returned by the function. Figure 2-2 shows the NPSS flowchart. The solid lines represent fluid ports while the dashed lines represent mechanical linkages between the turbomachinery and shafts. The dotted lines exiting the generators represent electrical output.

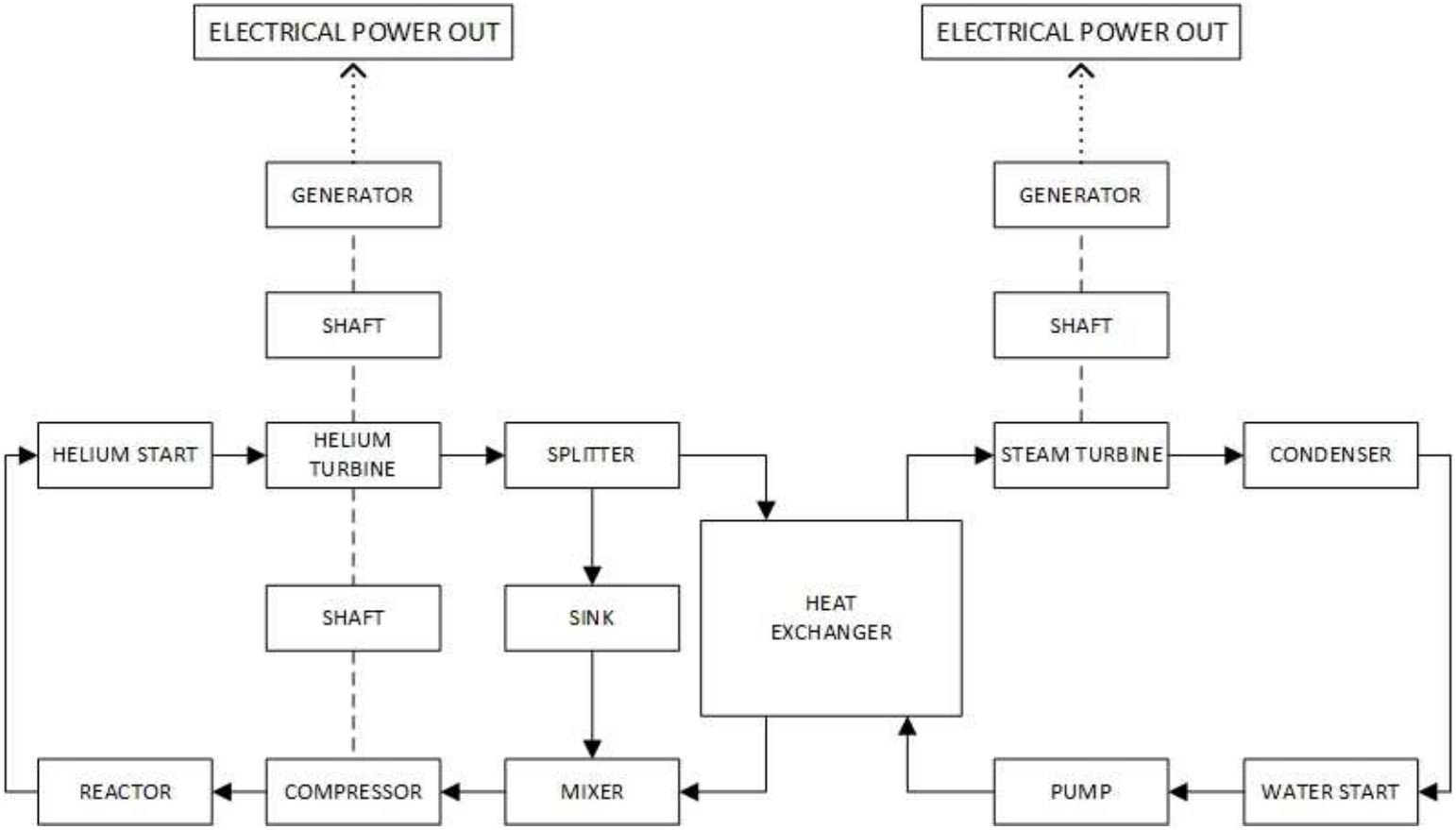

Figure 2-2 NPSS flowchart

Chapter 3

Brayton Cycle Sensitivity Studies

In this chapter, the effect of variation of Brayton cycle parameters is observed on the combined cycle. The parameters under consideration are the reactor outlet temperature, pressure loss through the reactor and polytropic efficiency of helium turbine and compressor.

3.1 Effect of Reactor Outlet Temperature

The reactor outlet temperature was varied to observe the effect on cycle parameters such as turbine pressure ratio, compressor pressure ratio and cycle efficiency. The turbine exit temperature was held constant at 753 K and the compressor inlet temperature was held constant at 326 K.

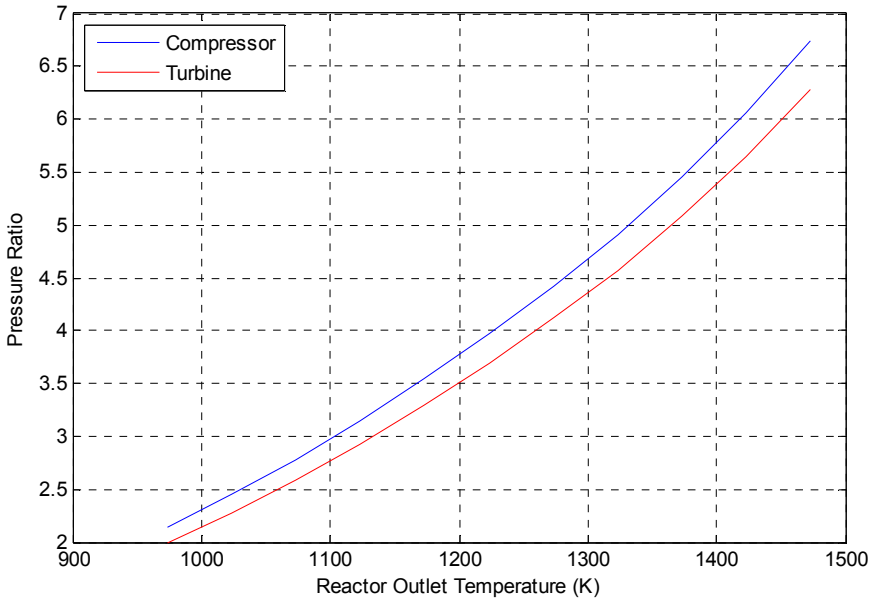

Figure 3-1 Variation of turbine and compressor pressure ratio with reactor outlet temperature

The variation in compressor and turbine pressure ratio with reactor temperature is seen in Figure 3-1. Due to the higher turbine inlet temperature, the turbine pressure ratio increases with reactor outlet temperature. In order to balance the pressure in the closed circuit, the compressor pressure ratio increases proportionately.

Figure 3-2 shows the variation of compressor and turbine adiabatic efficiency. The variation in adiabatic efficiency is because the turbine and compressor are assumed to have a design point polytropic efficiency of 92.8 percent and 90.5 percent respectively.

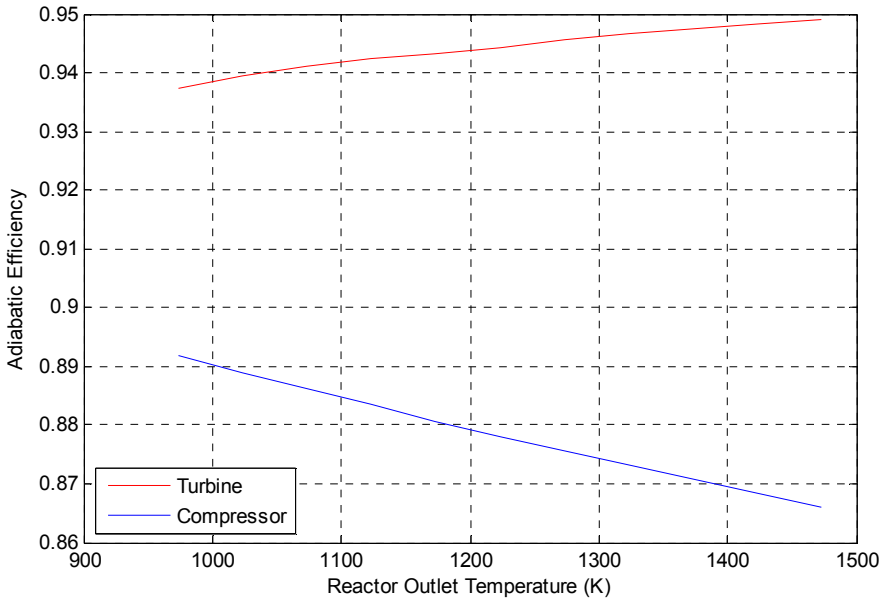

Figure 3-2 Variation of turbine and compressor efficiency with reactor outlet temperature

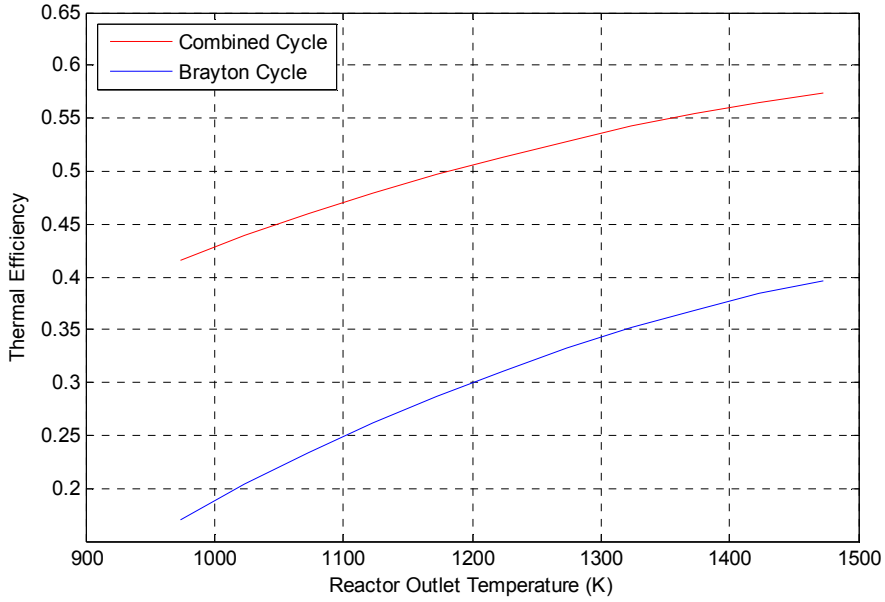

Figure 3-3 Variation of cycle efficiencies with reactor outlet temperature

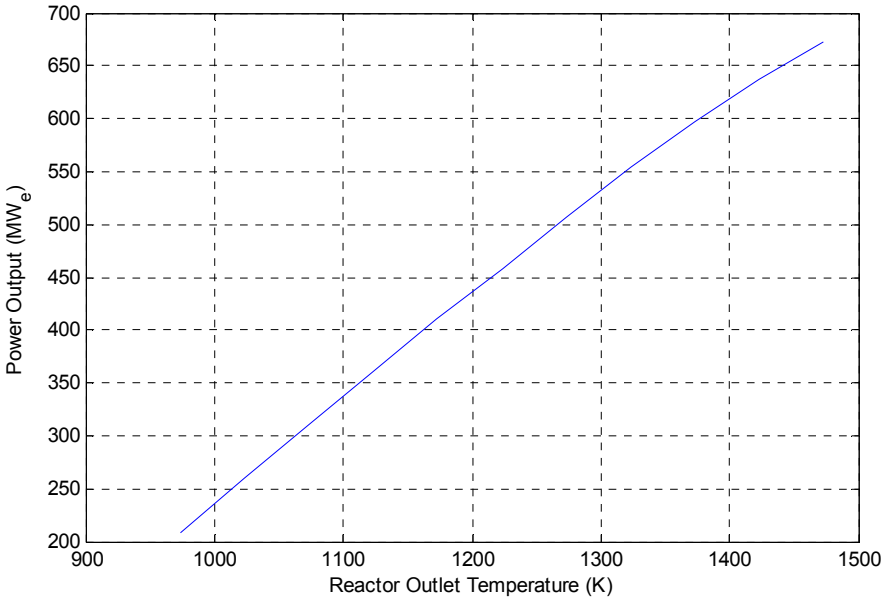

Figure 3-4 Variation of Brayton cycle output with reactor outlet temperature

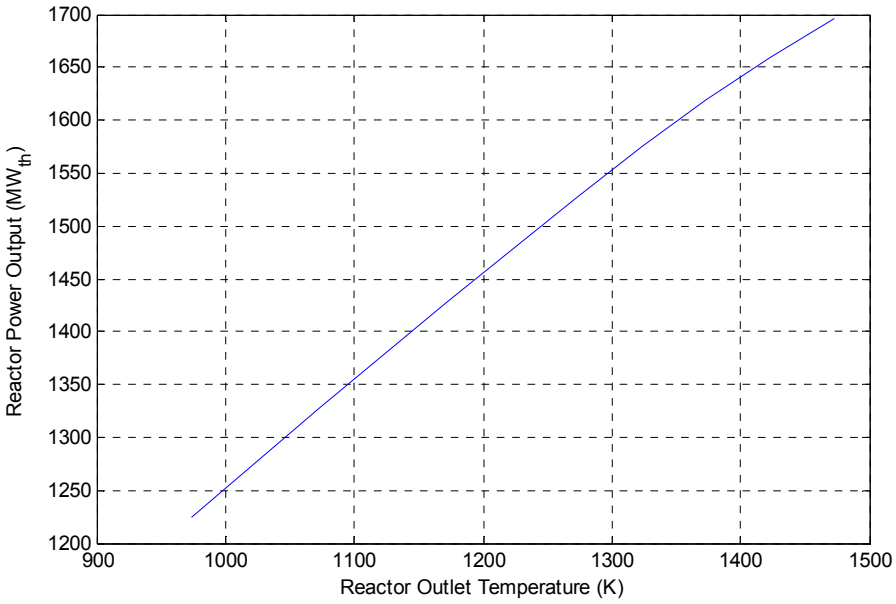

Figure 3-5 Variation of reactor power with reactor outlet temperature

Figure 3-3 shows the variation of Brayton cycle efficiency. As the turbine inlet temperature increases, the efficiency of the cycle increases resulting in a higher Brayton cycle power output as shown in Figure 3-4. In order to increase the reactor outlet temperature while keeping the mass flow rate constant, the reactor must produce more power. This is confirmed in Figure 3-5, which shows a steady increase in reactor thermal power with an increase in reactor outlet temperature.

The Rankine cycle efficiency does not vary with reactor power output as the steam temperature, pressure and mass flow rate do not change. But due to the increase in Brayton cycle efficiency, there is an increase in the combined cycle efficiency as seen in Figure 3-3. Table 3-1 summarizes the reactor outlet sensitivity data.

Table 3-1 Reactor Outlet Sensitivity Data

	Turbine			Compressor			Brayton		Combined Cycle	
Reactor Outlet	Pressure Ratio	Efficiency	Power	Pressure Ratio	Efficiency	Power	Power	Efficiency %	Reactor Power	Efficiency
K		%	MW		%	MW	MW_e	%	MW_{th}	%
1473	6.28	94.90	1713.7	6.74	86.59	1030.5	673.1	39.70	1695.6	57.39
1423	5.65	94.84	1595.1	6.06	86.83	948.5	636.9	38.39	1659.1	56.47
1373	5.08	94.76	1476.6	5.46	87.08	870.3	597.2	36.89	1618.7	55.42
1323	4.57	94.67	1358.0	4.91	87.31	795.7	553.8	35.17	1574.7	54.22
1273	4.12	94.56	1239.2	4.42	87.56	724.3	507.3	33.21	1527.4	52.85
1223	3.70	94.44	1120.6	3.97	87.81	654.8	458.8	31.03	1478.2	51.33
1173	3.30	94.33	1001.8	3.54	88.06	585.1	410.4	28.72	1429.1	49.71
1123	2.93	94.24	882.9	3.15	88.35	517.4	360.0	26.13	1377.9	47.90
1073	2.59	94.10	764.0	2.78	88.62	448.7	310.6	23.39	1327.8	45.98
1023	2.28	93.95	645.0	2.45	88.88	381.3	259.7	20.35	1276.2	43.86
973	2.00	93.74	526.0	2.14	89.19	314.7	208.1	17.00	1223.8	41.52

3.2 Variation of Reactor Pressure Loss

The pressure loss through the reactor was varied from 1 to 8 percent to observe its effect on cycle parameters. The reactor outlet temperature and pressure were kept constant at 1173 K and 6.89 MPa. The variation of compressor pressure ratio is seen in Figure 3-6. The increase in pressure ratio with reactor pressure loss is due to the turbine inlet pressure requirement. At higher pressure losses, as seen in Figure 3-7, the pressure entering the reactor has to be increased to have the desired turbine inlet pressure of 6.89 MPa. The increased pressure ratio results in a lower compressor adiabatic efficiency, as seen in Figure 3-8, as the compressor is designed based on a polytropic efficiency of 90.5 percent. The reduction in compressor efficiency causes the Brayton cycle efficiency to drop, as seen in Figure 3-9, thereby causing a drop in the combined cycle efficiency. The decrease in compressor efficiency also affects the Brayton cycle power output causing it to decrease as seen in Figure 3-10. The reactor power output is found to decrease with reactor pressure loss. Since the compressor pressure ratio increases so does the reactor inlet temperature, thereby reducing the amount of heat required to heat the helium to 1173 K.

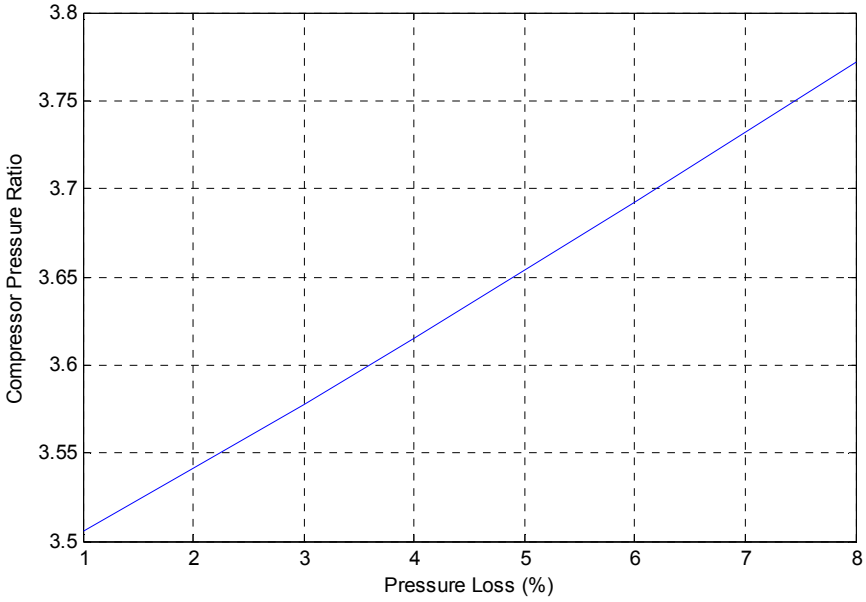

Figure 3-6 Variation of compressor pressure ratio with reactor pressure loss

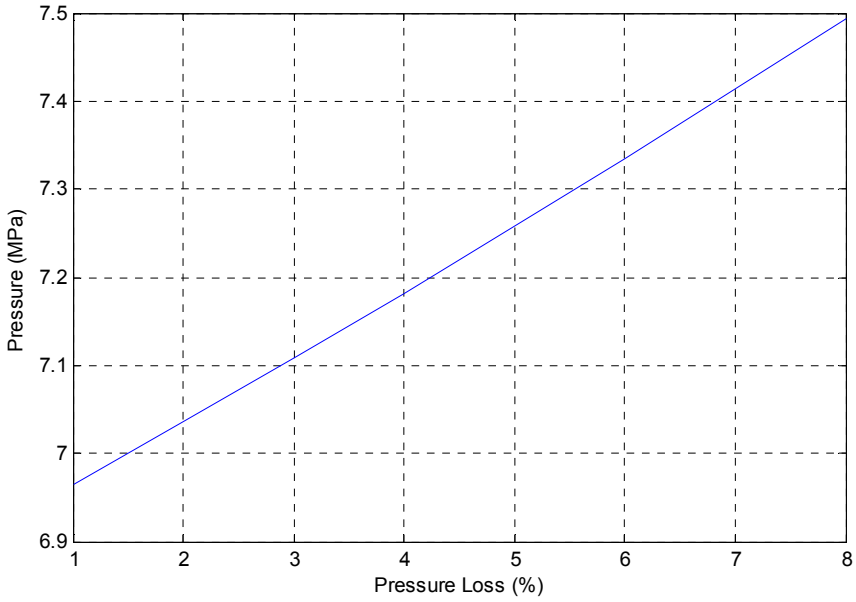

Figure 3-7 Variation of reactor inlet pressure with reactor pressure loss

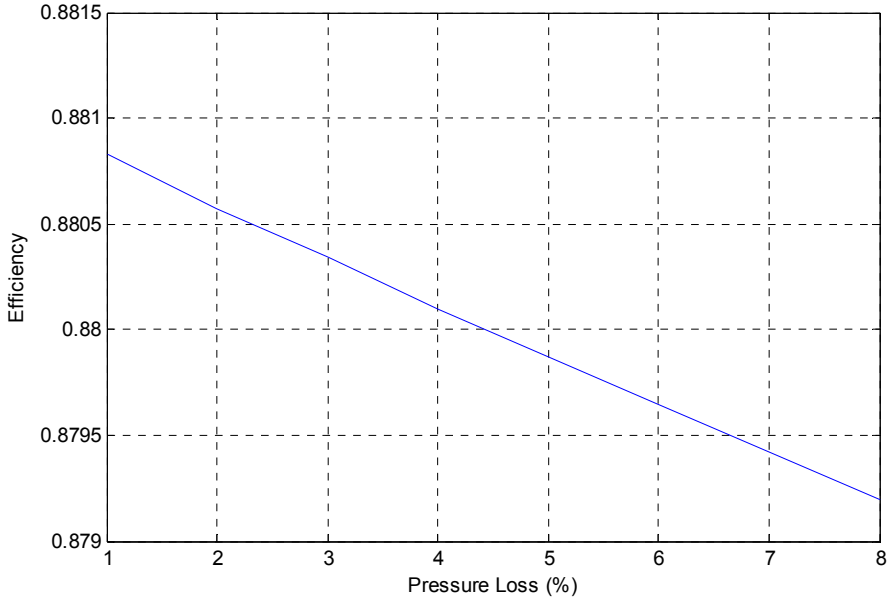

Figure 3-8 Variation of compressor adiabatic efficiency with reactor pressure loss

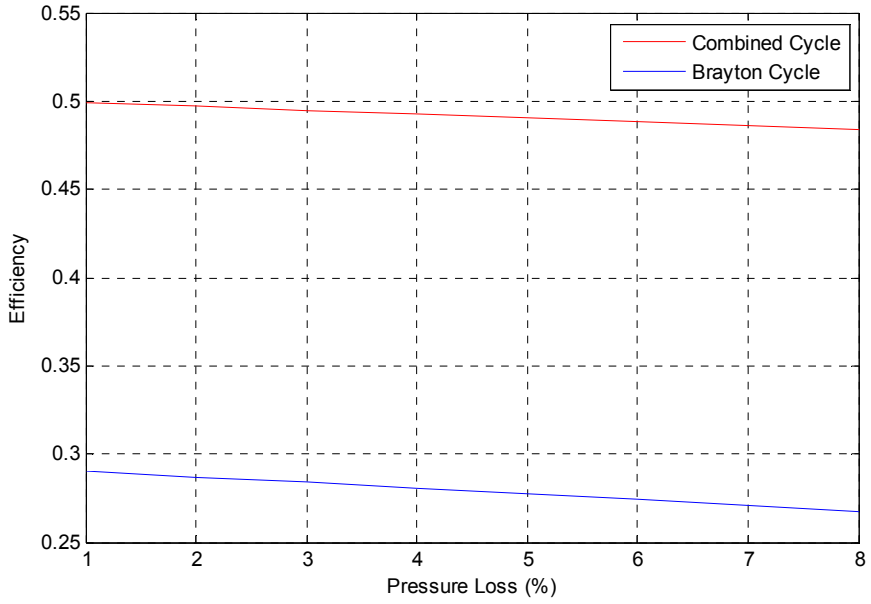

Figure 3-9 Variation of cycle efficiencies with reactor pressure loss

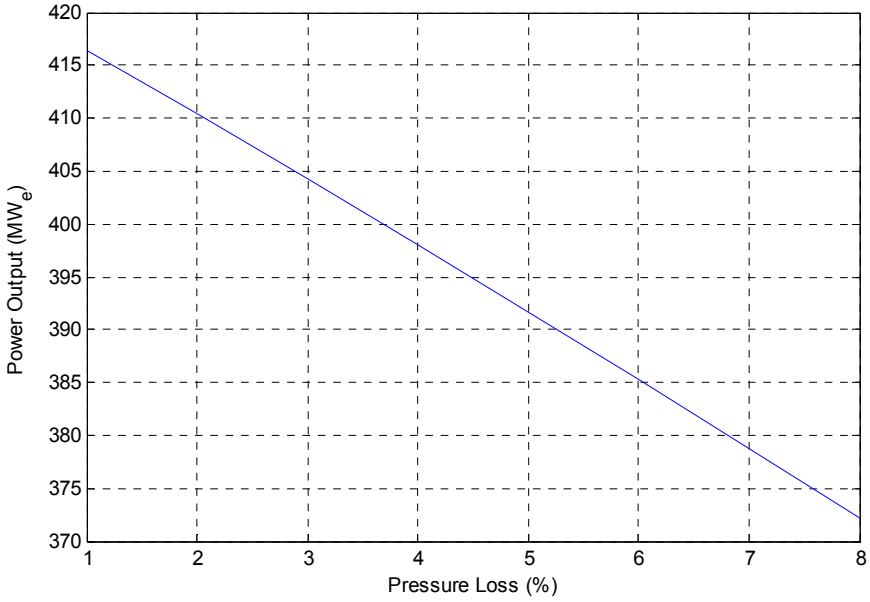

Figure 3-10 Variation of Brayton output power with reactor pressure loss

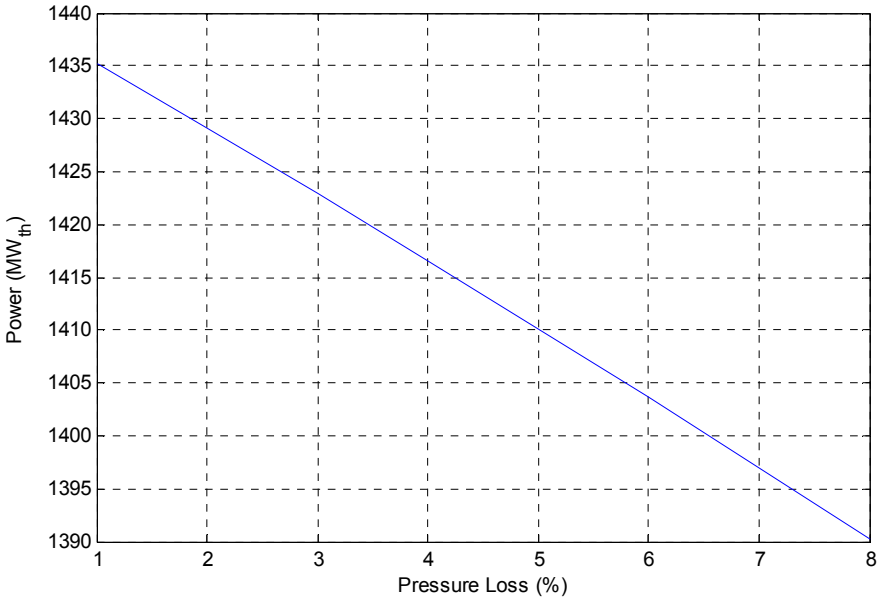

Figure 3-11 Variation of reactor power output with reactor pressure loss

3.3 Variation of Compressor Polytropic Efficiency

The effect of compressor polytropic efficiency on the components of the combined cycle plant is presented in this section. The compressor polytropic efficiency is varied from 95 percent to 85 percent and the effect of this variation is observed on the compressor output, reactor performance, and overall cycle performance. Table 3-2 summarizes this information.

Table 3-2 Compressor Polytropic Efficiency Study

Compressor				Reactor	Combined Cycle	
Polytropic Efficiency	Outlet Temperature	Adiabatic Efficiency	Power	Power	Efficiency	Power
%	K	%	MW	MW_{th}	%	MW_e
95	555	93.72	549.7	1464.5	50.89	745.3
94	558	92.46	557.2	1457.0	50.64	737.8
93	561	91.20	564.9	1449.3	50.39	730.3
92	565	89.95	572.8	1441.4	50.13	722.5
91	568	88.69	580.9	1433.3	49.85	714.5
90.5	570	88.06	585.1	1429.1	49.71	710.4
90	572	87.43	589.3	1424.9	49.56	706.3
89	575	86.17	597.9	1416.3	49.27	697.8
88	579	84.92	606.7	1407.5	48.96	689.1
87	583	83.66	615.8	1398.4	48.64	680.1
86	587	82.40	625.2	1389.0	48.30	670.9
85	591	81.15	634.9	1379.3	47.95	661.4

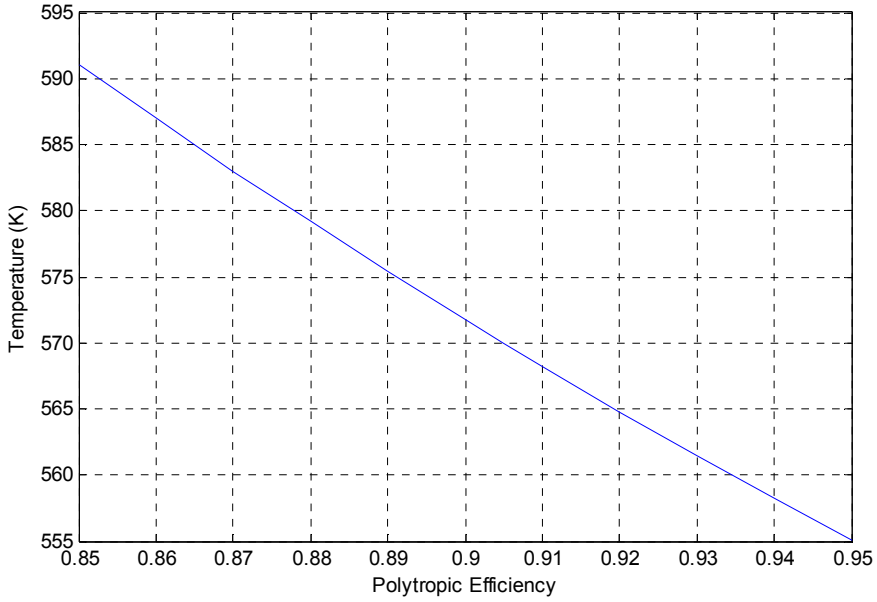

Figure 3-12 Variation of compressor outlet temperature with compressor polytropic efficiency

There is an increase in compressor outlet temperature as the compressor polytropic efficiency reduces as seen in Figure 3-12. The power required by the compressor also increases with reduction in polytropic efficiency and causes a reduction in Brayton cycle power as seen in Figure 3-13. The corresponding reduction in combined cycle efficiency is seen in Figure 3-14. The turbine is not affected by the variation in compressor efficiency as the compressor and reactor are constrained to provide the turbine with helium at a specific temperature and pressure.

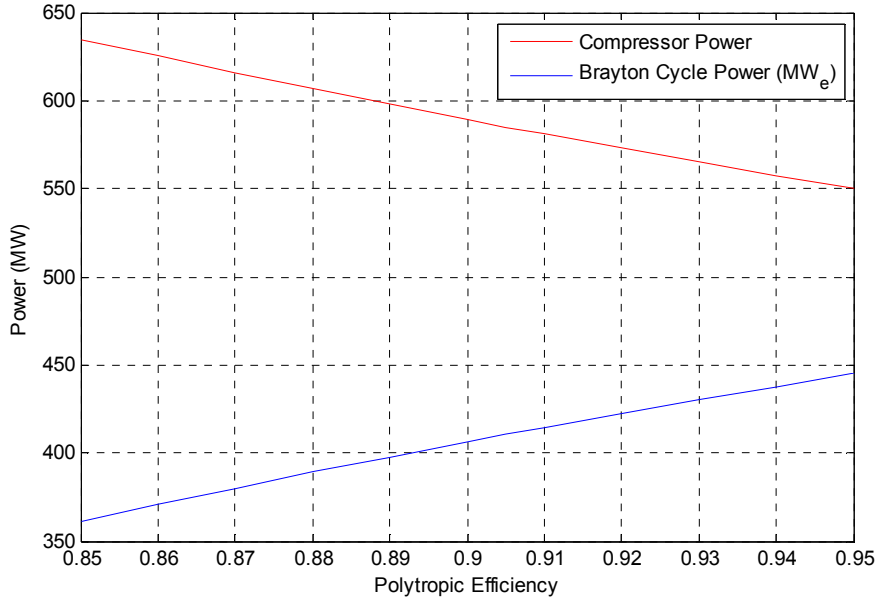

Figure 3-13 Variation of Brayton cycle and compressor power with compressor polytropic efficiency

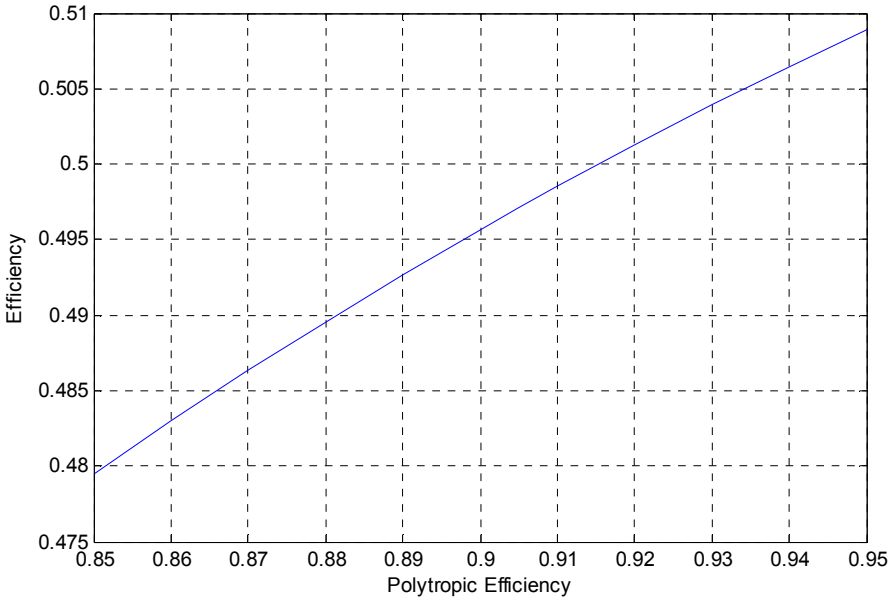

Figure 3-14 Variation of combined cycle efficiency with compressor polytropic efficiency

3.4 Variation of Turbine Polytropic Efficiency

In this final section, we observe the effect of turbine polytropic efficiency on the components of the combined cycle. The turbine polytropic efficiency is varied from 95 percent to 85 percent. Table 3-3 contains the turbine and compressor values.

As the turbine is required to expand the flow to 753 K, a decrease in turbine polytropic efficiency causes the turbine pressure ratio to increase as seen in Figure 3-15. Due to the higher turbine expansion ratio, the compressor pressure ratio increases to meet the reactor inlet pressure requirement. The higher compressor pressure ratio causes the compressor outlet temperature to increase as seen in Figure 3-16.

As seen in Figure 3-17, the power required by the compressor increases due to the higher pressure ratio required, thereby lowering the combined cycle output power. The higher compressor outlet temperature requires a lower reactor power output to meet the 1173 K outlet temperature requirement. Due to the combined effect of reduction of turbine polytropic efficiency on the combined cycle components, there is a reduction in the overall combined cycle efficiency as seen in Figure 3-18.

Table 3-3 Turbine Polytropic Efficiency Study

Turbine				Compressor				Combined Cycle		
Polytropic Efficiency	PR	Efficiency	Power	PR	Efficiency	Temperature	Power	Power	Efficiency	Reactor Power
%		%	MW		%	K	MW	MW_e	%	MW_{th}
95	3.20	96.11	1001.68	3.44	88.12	563	567.7	427.5	50.29	1446.5
94	3.25	95.31	1001.71	3.48	88.10	566	575.3	420.0	50.04	1438.8
93	3.29	94.49	1001.74	3.53	88.06	569	583.4	412.1	49.77	1430.8
92.8	3.30	94.33	1001.75	3.54	88.06	570	585.1	410.4	49.71	1429.1
92	3.34	93.68	1001.77	3.58	88.03	573	591.8	403.8	49.48	1422.4
91	3.38	92.90	1001.83	3.63	88.00	576	599.7	396.1	49.21	1414.6
90	3.43	92.11	1001.86	3.68	87.97	580	608.0	388.0	48.92	1406.4
89	3.47	91.32	1001.91	3.73	87.94	583	616.4	379.7	48.62	1397.9
88	3.52	90.53	1001.95	3.78	87.91	587	625.1	371.2	48.31	1389.4
87	3.58	89.74	1002.00	3.84	87.88	591	634.3	362.2	47.98	1380.2
86	3.63	88.96	1002.05	3.89	87.85	595	643.4	353.3	47.65	1371.1
85	3.68	88.17	1002.09	3.95	87.81	599	653.0	343.9	47.29	1361.6

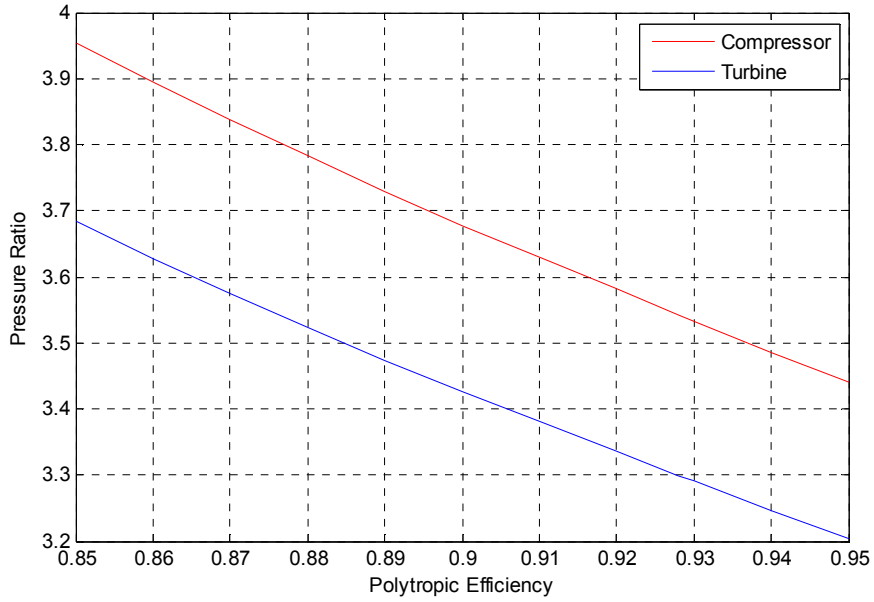

Figure 3-15 Variation of turbine and compressor pressure ratio with turbine polytropic efficiency

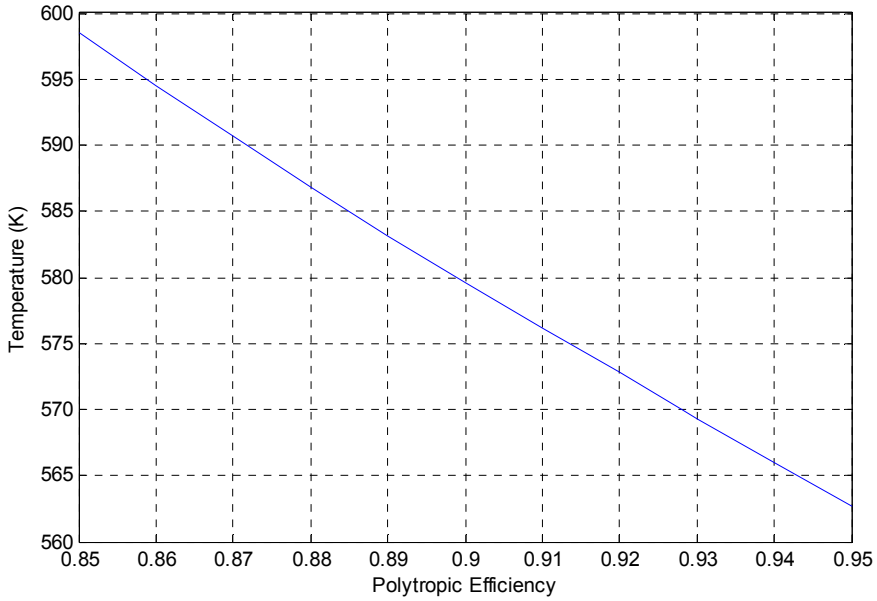

Figure 3-16 Variation of compressor exit temperature with turbine polytropic efficiency

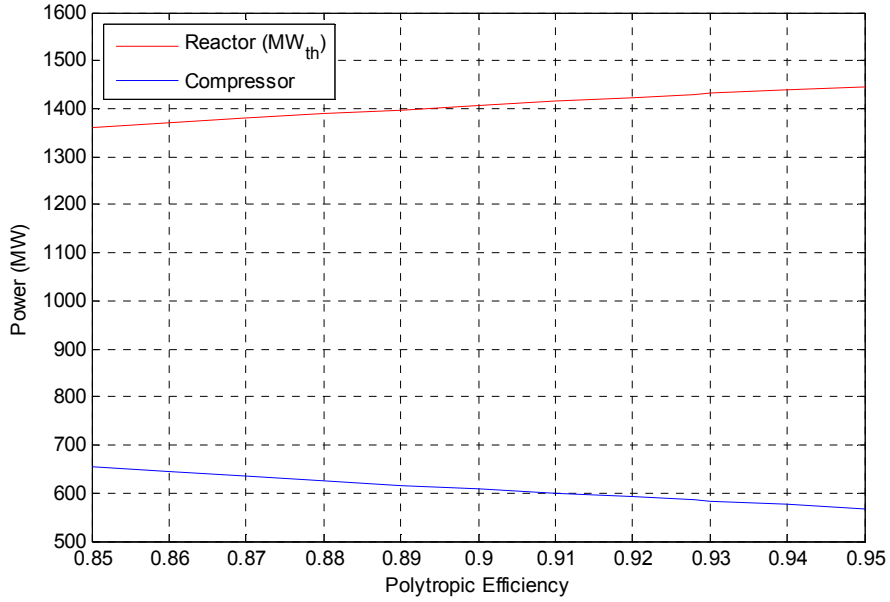

Figure 3-17 Variation of compressor power and reactor power with turbine polytropic efficiency

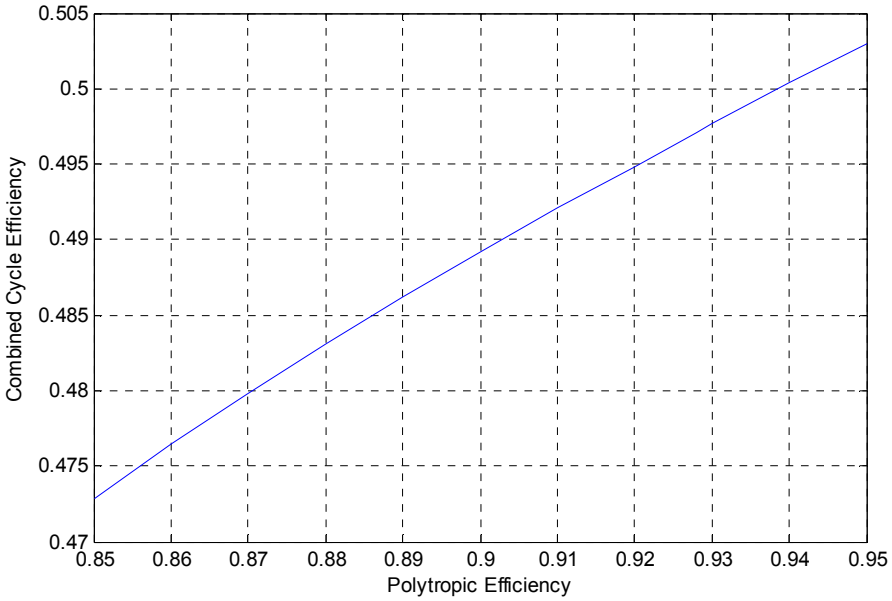

Figure 3-18 Variation of combined cycle efficiency with turbine polytropic efficiency

Chapter 4

Simulation of Design Point and Part-Load Performance

This chapter discusses the procedure followed and the assumptions made while setting up the design point and part load simulation. The NPSS solver uses a set of independent and dependent variables that is declared by the elements and the user. The independents are varied with each solver iteration until the dependent variables satisfy their specified condition [21].

The heat rise element, i.e. nuclear reactor is modeled in such a way that the temperature of helium exiting the reactor and entering the helium turbine is maintained at 1173 K. During part load operation of the Brayton cycle, the mass flow rate is reduced. By reducing the reactor power output, the temperature of helium can be maintained at the design point value. Load following can be carried out by both Brayton and Rankine cycles. Both cases are analyzed in this chapter.

4.1 Design Point

Setting the design point of the combined cycle plant relies on the configuration of the existing steam cycle. The Brayton cycle is sized based on the quality and quantity of steam required by the steam turbine. When the heat source is changed from burning coal to the helium turbine exhaust, we must ensure that the turbine exhaust has sufficient thermal energy to generate the required steam.

For the 300 MW_e steam plant currently under analysis, steam is required at 723 K, 10.34 MPa and a mass flow rate of 330 kg/s. The steam turbine extracts 312.5 MW of power at 84 percent adiabatic efficiency. With the generator loss at 4 percent, the electrical output is 300 MW_e. A mechanical pump is used to pump the water

into the heat exchanger where it absorbs the heat from the helium turbine exhaust before entering the steam turbine. Design point specifications are given in Table 4-1.

Table 4-1 Steam Cycle Design Point Specifications

Heat Exchanger	Water In (K)	312
	Water Pressure In (MPa)	10.66
	Pressure Loss (%)	3
Steam Turbine	Mass Flow Rate (kg/s)	330
	Inlet Temperature (K)	723
	Inlet Pressure (MPa)	10.34
	Exit Steam Quality	0.86
	Exit Pressure (kPa)	2.06
	RPM	3600
	Pressure Ratio	500
	Adiabatic Efficiency (%)	84.0
	Power Out (MW)	312.5
Generator	RPM	3600
	Power In (MW)	312.5
	Power Out (MW_e)	300
	Efficiency (%)	96
Pump	Pressure Ratio	531.4
	Power (kW)	4417
	RPM	3600

The development of ceramic structural materials like SiC_f/SiC for use in reactors allow a maximum temperature of 1473 K [21]. Due to the possibility of Nuclear Regulatory Commission restrictions on reactor outlet temperature, a reactor temperature

of 1173 K was selected. The work done by Tiwari, et al. [22] shows that increasing the pressure ratio of the helium turbine results in a lower turbine exit temperature (TET). In the work by Camporeale, et al. [23], the minimum temperature difference on each side of the heat exchanger was assumed to be 10 K. The helium turbine pressure ratio was configured to obtain a TET of 753 K. Hence the temperature difference at the hot side of the heat exchanger was 30 K. Adopting a similar approach at the cold side; the heat exchanger effectiveness was lowered to 97.4 percent to allow for a temperature difference of at least 14 K. The mass flow rate of helium that was required to satisfy the heat exchanger requirements was calculated to be 456.36 kg/s.

The compressor pressure ratio was selected based on the turbine pressure ratio, pressure loss in the reactor [24] and pressure losses in other elements such as the heat exchanger and the sink. The result was a helium cycle power output of 416.67 MW_e. After assuming a 1.5 percent conversion loss between the turbine and the generator the electrical output was measured at 410.41 MW_e. The entire helium system was pressurized to maintain sufficient density for efficient operation [25].

4.2 Brayton Part Load Performance

Part load operation of the Brayton cycle can be implemented as a means of load following when there is an anticipated drop in power demand. To simulate the Brayton part load performance, the reactor outlet temperature is held constant while reducing reactor output power. This is done by reducing the mass flow rate of helium through the reactor core as the reactor power is reduced. Thus, the turbine sees a constant inlet temperature. Two assumptions are made while simulating the part load performance of the Brayton cycle. First, the flow into the turbine is choked, meaning the flow is travelling at or near transonic conditions [26]. The simplified equation of mass flow at off-design is given by:

$$m_{OD}\frac{\sqrt{T4_{OD}}}{P4_{OD}} = m_{DP}\frac{\sqrt{T4_{DP}}}{P4_{DP}}$$

Assuming that the temperature of helium out of the reactor is maintained constant, the equation further reduces to:

$$m_{OD} = m_{DP}\frac{P4_{OD}}{P4_{DP}}$$

The second assumption is that of constant volumetric flow rate across the compressor [26]. In order to maintain synchronous speeds with the gas turbine while still reducing or increasing power output, the engine must be properly controlled [26]. *"The control of the engine depends on where in the part-load curve the engine is operating"* [26].

A reduction in mass flow rate causes the compressor pressure ratio and efficiency to drop [26]. As the mass flow rate is reduced, the turbine exhaust gas temperature increases to maintain energy balance [26]. The mass flow rate of helium can be decreased to a limit until either material restrictions at the turbine exit or heat exchanger inlet prohibit the higher temperatures [26] or the efficiency of the turbomachinery falls below an acceptable level.

There is a coupling effect between the two systems when the Brayton cycle is operated at part load. The coupling occurs due to two constraints; helium must be cooled to its design point temperature after passing through the heat exchanger and the temperature of steam entering the turbine must be maintained at its design point temperature. The solver calculates the new mass flow rate of water required to cool the helium. The change in mass flow rate of steam due to the reduction of Brayton cycle mass flow rate causes a change in the Rankine cycle power output.

4.3 Rankine Part Load Performance

Part load operation of the Rankine cycle can be implemented as a means of load following when there is a fluctuation in power demand over a short time period. The ability to quickly vary the mass of steam allows the system to rapidly change the power produced.

The Rankine cycle part load operation follows a similar setup as the Brayton cycle part load operation, except that there is no change in helium mass flow rate resulting in the Brayton cycle operating at design point. Since the water pump is not connected directly to the steam turbine, it can be controlled independently. The rpm of the pump is varied to obtain the required steam pressure and mass flow rate into the steam turbine. The off design performance of the steam turbine is calculated by the steam turbine map file.

While the Brayton cycle runs at the design point, due to the reduction in Rankine cycle mass flow rate, the helium entering the heat exchanger has more thermal energy than is required by the Rankine cycle. The required amount of helium is passed through the heat exchanger and the remaining helium is bypassed. In order to cool the helium to its design point value, the bypassed helium is then passed through a sink. By rejecting heat at the sink and bringing the temperature of helium to its design point value, there is less stress on the compressor caused by temperature variations. The flow is then combined and sent to the compressor, where the cycle begins again.

Chapter 5

Results

This chapter summarizes the results obtained from the NPSS simulation of the combined cycle power plant at design and part load operation. As described in the previous chapter, setting the design of the Brayton cycle depends largely on the requirements of the steam cycle followed by the requirements of the heat exchanger. At both design point and part load, the turbomachinery is maintained at a synchronous speed of 3600 rpm.

5.1 Design Point

Table 4-1 provides the design point specification of the combined cycle plant. At design point, the reactor power requirement is estimated at 1429.14 MW_{th}. From the viewpoint of utilization of pebble bed reactors that are under development, three 500 MW_{th} reactors would be required to power to the entire system. At design point, the Brayton cycle has an efficiency of 28.71 percent and the Rankine cycle has an efficiency of 29.63 percent. The resulting combined cycle has an efficiency of 49.71 percent.

The mass flow rate of helium required at design point is 456.36 kg/s. The design point helium compressor adiabatic efficiency is 88.05 percent and 585.1 MW of power is required for a compressor pressure ratio of 3.54. The helium turbine generates 1001.8 MW of power at a pressure ratio of 3.29 and has an adiabatic efficiency of 94.33 percent. The adiabatic efficiencies of the turbine and compressor were calculated based on a turbine polytropic efficiency of 92.8 percent and compressor polytropic efficiency of 90.5 percent [11]. At a generator loss of 1.5 percent, the electrical power obtained from the Brayton cycle is 410.42 MW_e. Table 4-1 summarizes some cycle design point values.

Table 5-1 Design Point Values of Combined Cycle Turbomachinery

Brayton Cycle								
Compressor	Pressure Ratio	3.54	Helium Turbine	Pressure Ratio	3.29	Generator	Power In (MW)	416.7
	Efficiency %	88.05		Efficiency %	94.33		Torque In (kN-m)	1105.2
	Power (MW)	585.1		Power (MW)	1001.8		Power Out (MW_e)	410.4
	Torque (kN-m)	1551.9		Torque (kN-m)	2657.2		Torque Out (kN-m)	1088.7
Rankine Cycle								
Water Pump	Pressure Ratio	531.31	Steam Turbine	Pressure Ratio	500	Generator	Power In (MW)	312.5
	Power (kW)	4417		Efficiency%	84		Torque In (kN-m)	828.9
	RPM	3600		Power (MW)	312.5		Power Out (MW_e)	300
				Torque (kN-m)	828.9		Torque Out (kN-m)	795.8

5.2 Brayton Part Load

In the Brayton cycle, we reduce or increase the mass flow rate of helium through the Brayton circuit by using the helium tank. Since the power output of the Brayton cycle is directly related to the mass flow rate, we observe the effect of reduction in power on mass flow rates, pressure ratios, helium turbine outlet temperatures and cycle efficiencies.

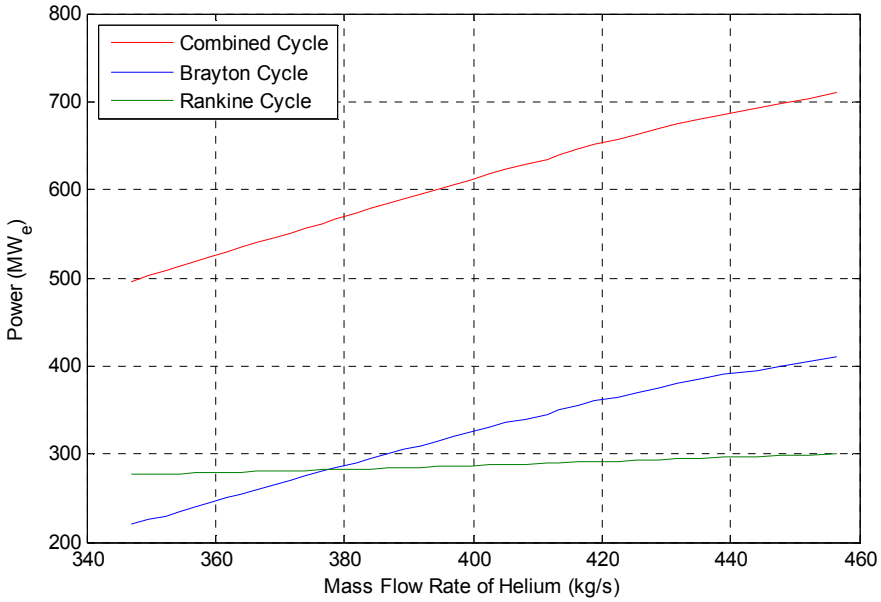

Figure 5-1 Variation of combined cycle power, Brayton cycle power and Rankine cycle power with helium mass flow rate

The trends in variation of cycle power, Brayton power and Rankine power versus helium mass flow rate are shown in Figure 5-1. The mass flow rate of helium was reduced to 346.92 kg/s, 76 percent of the design point value. As the mass flow rate of helium was reduced through the system, the power output of the Brayton cycle reduced almost linearly at a rate of 1.76 MW_e per kg/s of helium mass flow rate. Due to closed

cycle coupling, the systems are not independent and it was found that the Rankine power dropped at a rate of 0.22 MW_e per kg/s of helium mass flow rate reduced. As seen in Figure 5-2 the heat that is transferred from the Brayton cycle to the Rankine cycle reduces with reduction in Brayton mass flow rate. The reduction in Rankine power is due to the reduction in mass flow rate of water that is being pumped to maintain the required quality of steam.

As the mass flow rate of helium is reduced for part load operation of the Brayton cycle, the temperature at the turbine exit increases as seen in Figure 5-3. As discussed in the previous chapter, this happens to maintain the energy balance. The mass flow rate can be decreased for part load operation until the turbine exit temperature reaches its limit [26].

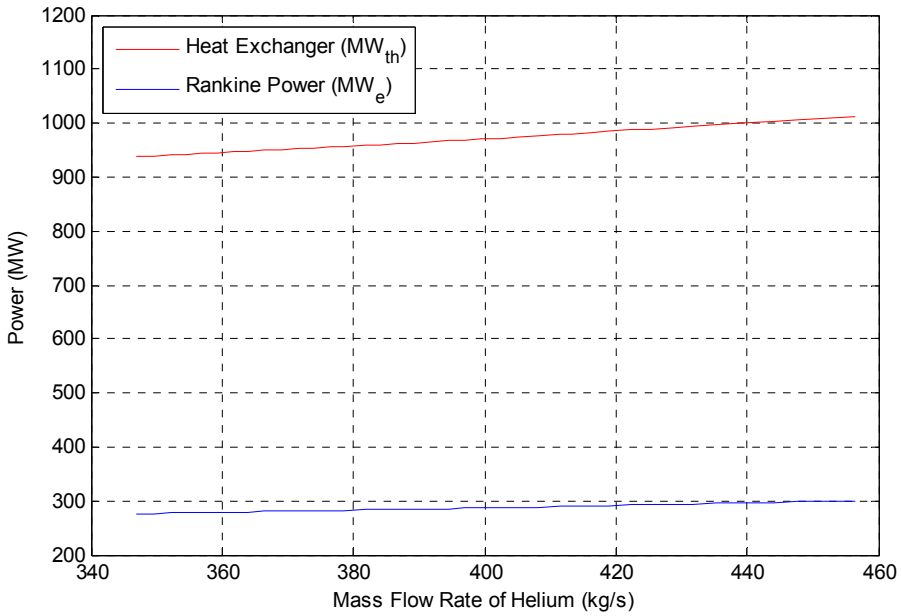

Figure 5-2 Variation of Rankine cycle power and condenser heat with helium mass flow rate

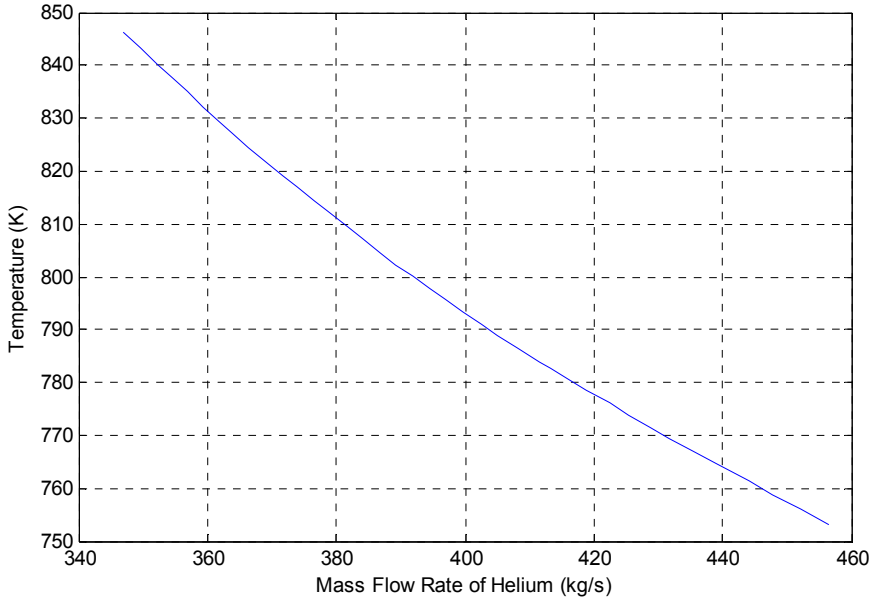

Figure 5-3 Variation of helium turbine exit temperature with helium mass flow rate

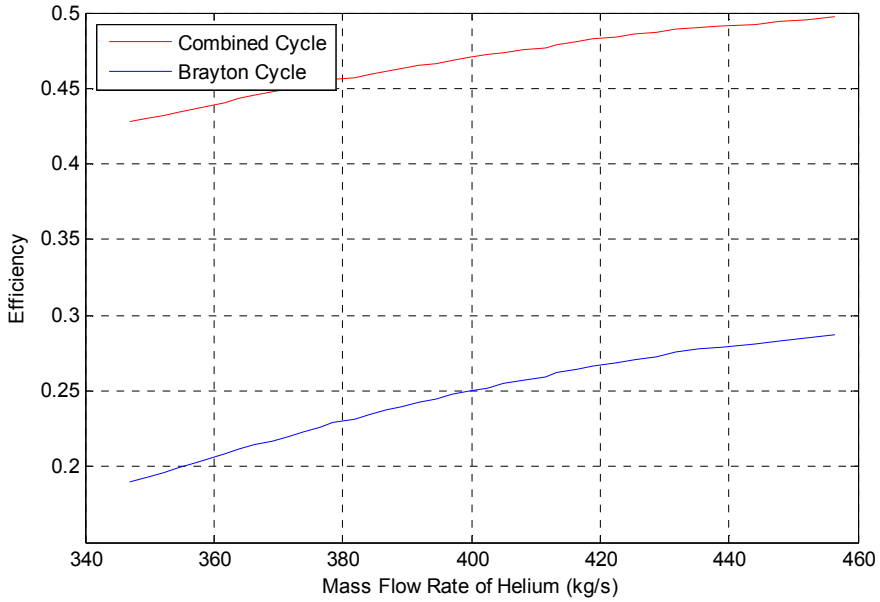

Figure 5-4 Variation of Brayton and combined cycle efficiency with helium mass flow rate

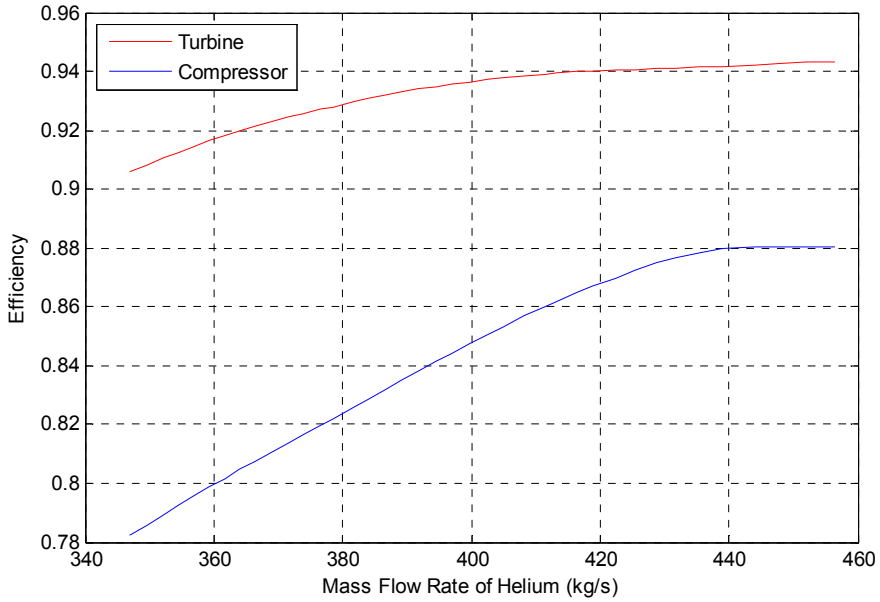

Figure 5-5 Variation of turbine and compressor adiabatic efficiencies with helium mass flow rate

The Brayton cycle efficiency reduces as the mass flow rate of helium is reduced through the system as shown in Figure 5-4. The cycle efficiency drop is a result of a reduction in efficiency in the turbine and compressor. Figure 5-5 shows the trends in reduction of turbine and compressor efficiencies for a reduction in helium mass flow rate. This trend is based on the GTHTR300 helium turbomachinery. Figure 5-6 shows the variation of pressure ratios of the helium turbomachinery during part load operation.

As seen in Figure 5-7, in order to maintain the reactor outlet temperature at 1173 K, the reactor power would have to be reduced almost linearly with the mass flow rate of helium.

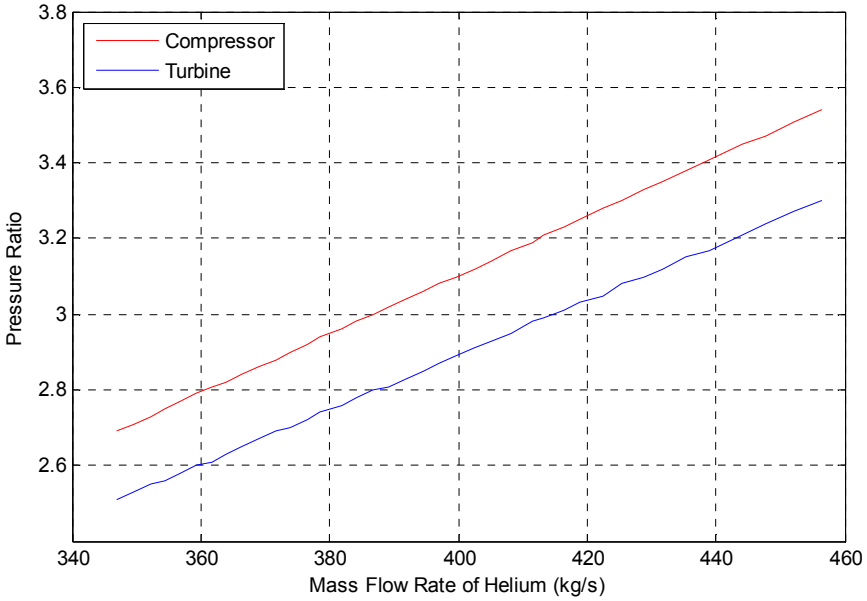

Figure 5-6 Variation of turbine and compressor pressure ratios with helium mass flow rate

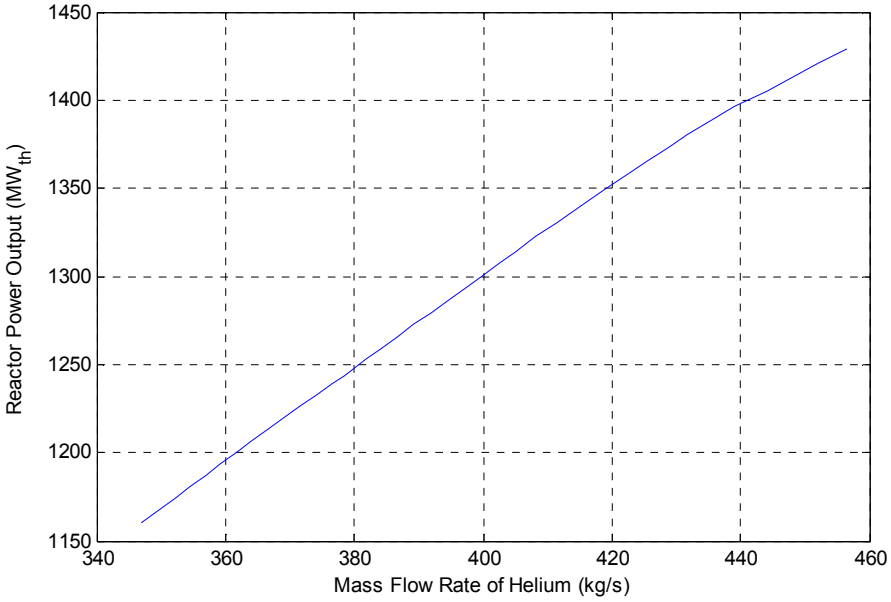

Figure 5-7 Variation of reactor output with helium mass flow rate

5.3 Rankine Part Load

As discussed in the previous chapter, the part load operation of the Rankine cycle is carried out while keeping the Brayton cycle running at design point. The pump rpm, as seen in Figure 5-8, and power required by the pump, as seen in Figure 5-9 decreases linearly as Rankine cycle power output is reduced.

The steam turbine inlet pressure, as seen in Figure 5-10, and mass flow rate of steam, as seen in Figure 5-11, is also reduced linearly as the Rankine power drops. As the steam pressure into the turbine is reduced, the turbine pressure ratio falls as seen in Figure 5-12. Unlike during the Brayton cycle part load operation, the temperature of steam at the exit of the turbine, during the Rankine cycle part load operation, remains constant. This is due to the fact that steam at the turbine exit is in a two phase state and instead of temperature, the quality of steam at the exit of the turbine, as shown in Figure 5-13, increases as the power is reduced.

The drop in turbine adiabatic efficiency of the steam turbine with the reduction in Rankine power output, as seen in Figure 5-14, can be attributed to the off-design performance characteristics of the turbine which is operating at a reduced inlet pressure and mass flow rate. Running the Rankine cycle at part load, while operating the Brayton cycle at design point, as discussed in the previous chapter, reduces the energy required by the steam. Due to the heat exhausted in the sink during part load operation of the Rankine cycle, there is a decrease in overall cycle efficiency as shown in Figure 5-15. The variation of mass flow rate through the heat exchanger and bypassed mass flow rate during part load operation of the Rankine cycle is seen in Figure 5-16.

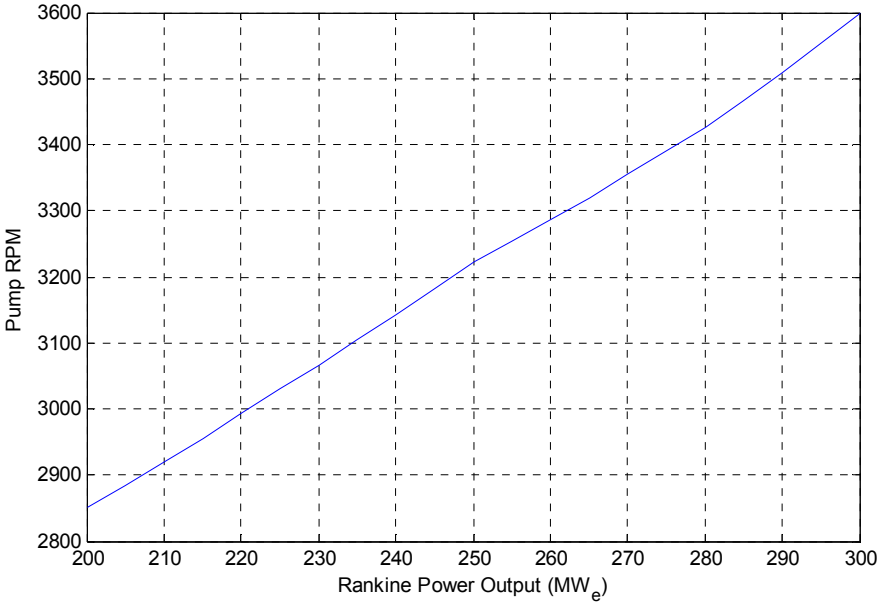

Figure 5-8 Variation of pump RPM with Rankine power output

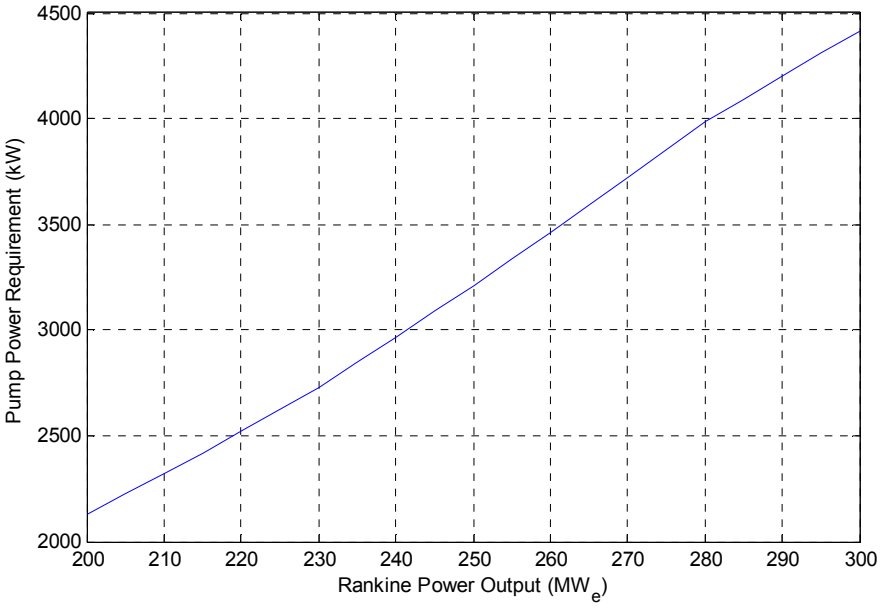

Figure 5-9 Variation of pump power requirement with Rankine power output

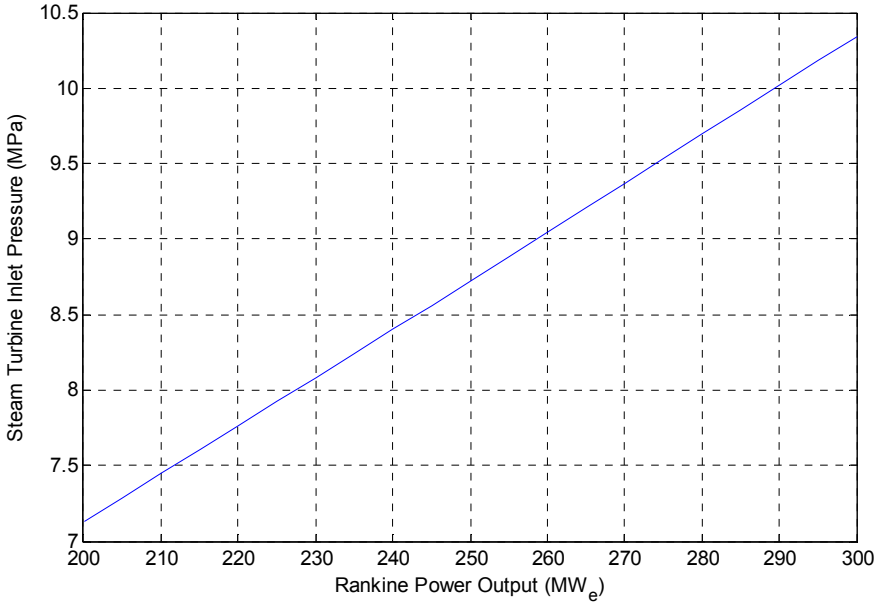

Figure 5-10 Variation of turbine inlet pressure with Rankine power output

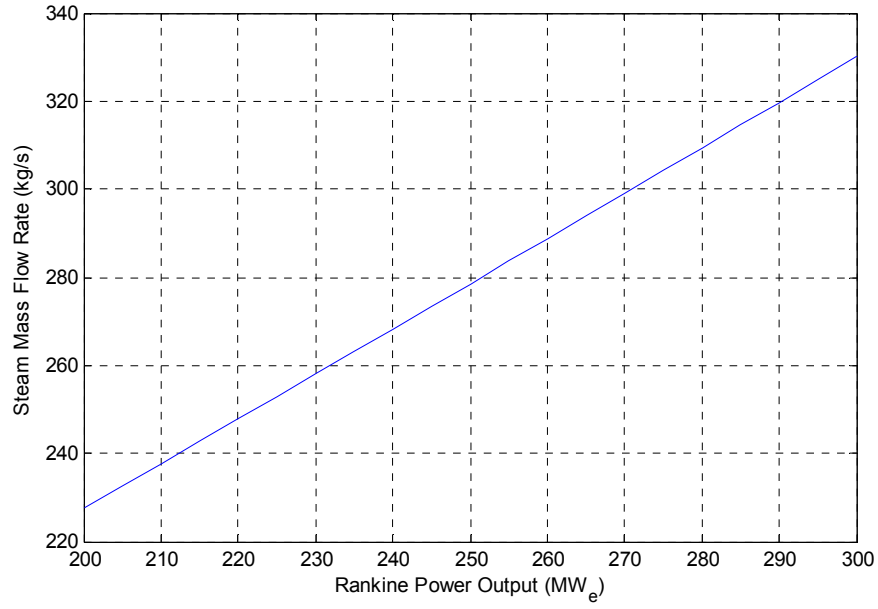

Figure 5-11 Variation of steam mass flow rate with Rankine power output

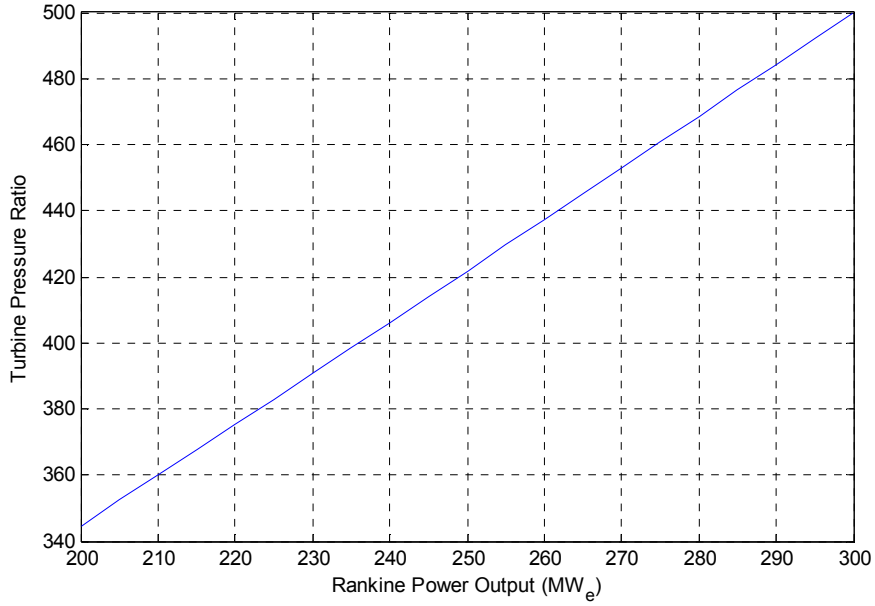

Figure 5-12 Variation of turbine pressure ratio with Rankine power output

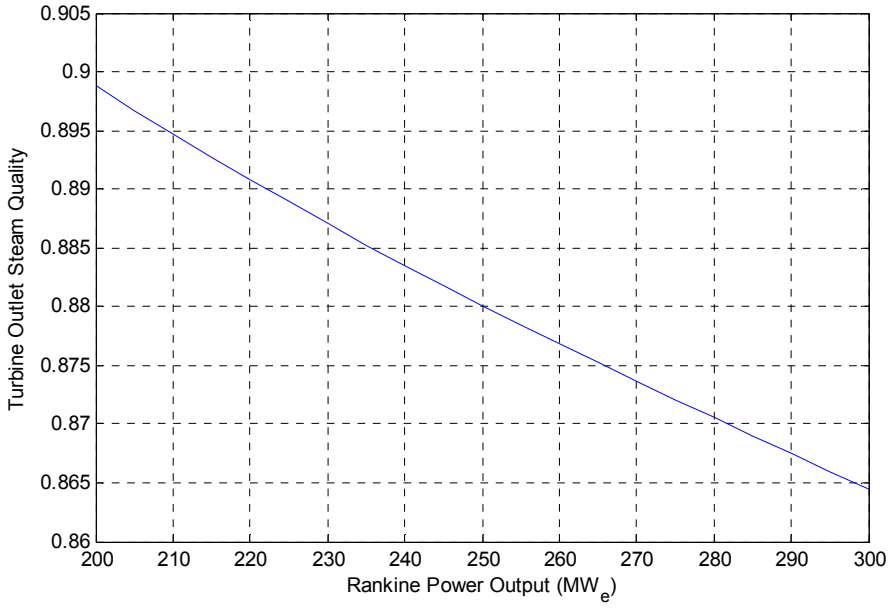

Figure 5-13 Variation of steam quality at turbine outlet with Rankine power output

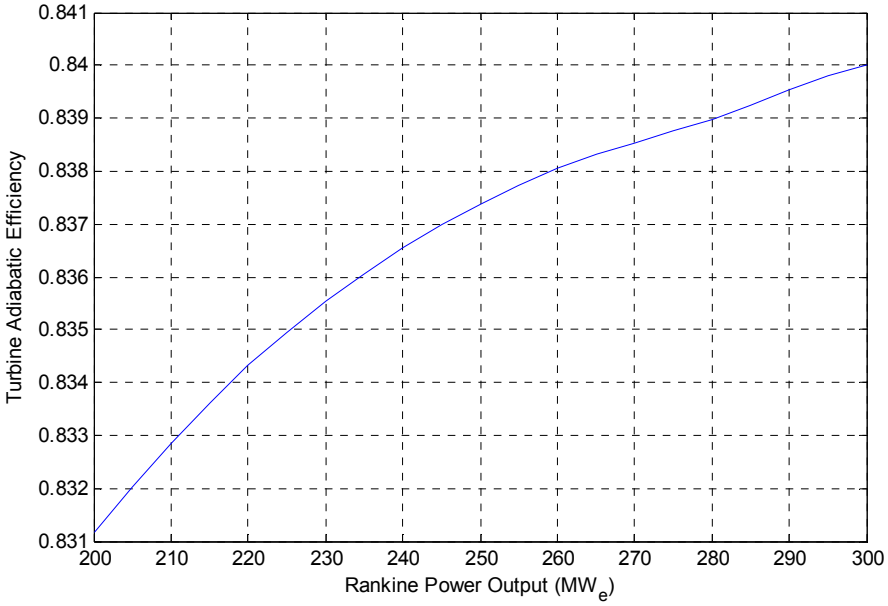

Figure 5-14 Variation of turbine adabatic efficiency with Rankine power output

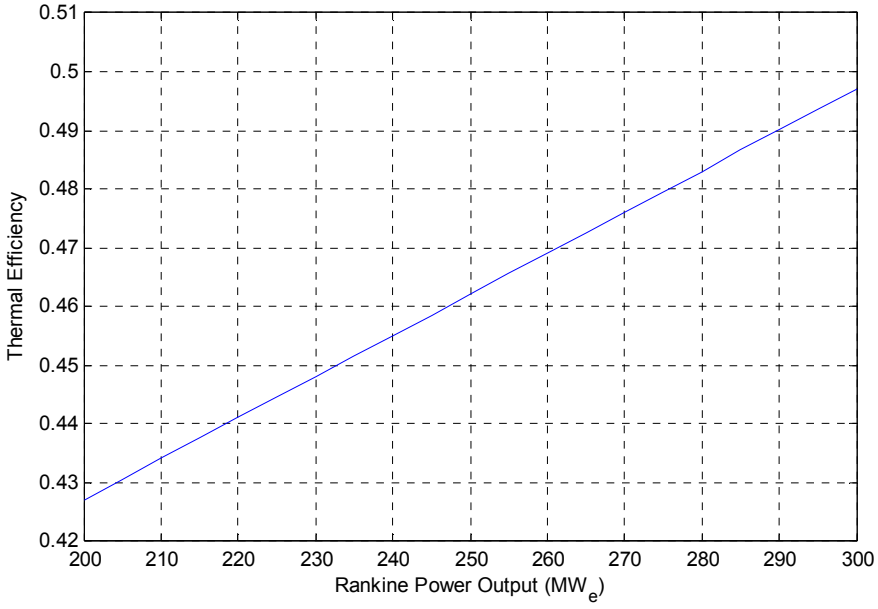

Figure 5-15 Variation of combine cycle efficiency with Rankine power output

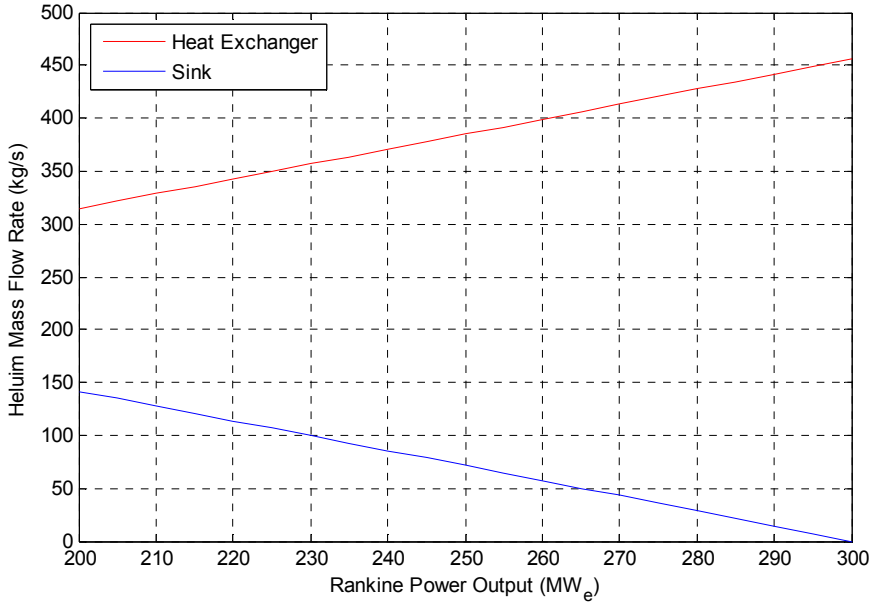

Figure 5-16 Variation of mass flow rate through heat exchanger and sink with Rankine power output

Chapter 6

Conclusions and Future Research

This chapter summarizes the work done in this research and contains suggestions for future research.

6.1 Conclusions

The main goal of this research was to develop a system to setup and calculate the design point configuration of a Brayton cycle that could serve as a topping unit and power an existing 300 MW_e steam cycle. This research would provide a method to overhaul ageing coal power plants, providing electricity at higher efficiency and lowering CO_2 emissions. The combined cycle plant produces a power of 710.4 MW_e with an efficiency of the 49.71 percent, an improvement over the existing steam cycle that produced 300 MW_e at an efficiency of 29.63 percent. From the latest U.S. Department of Energy figures [27], an equivalent 710 MW_e coal plant would produce 5.84 million tonnes of CO_2 every year and a natural gas plant would produce 3.42 million tonnes of CO_2 every year.

The use of NPSS permits the analysis of turbomachinery at various levels of complexity. With the turbomachinery performance maps, the system can be evaluated for part load and off-design performance. NPSS provides the opportunity to quickly analyze the effect of minor changes, thereby providing the opportunity to quickly adapt and optimize the cycle.

The feasibility of a recuperated helium cycle was analyzed briefly. The recuperated cycle provided a higher Brayton cycle efficiency by capturing the exhaust heat from the helium turbine before sending it to the heat exchanger. However, the

helium entering the heat exchanger was at a much lower temperature than required by the steam cycle. Hence the use of a recuperator was ruled out.

6.2 Future Research

The current design is based around an existing steam cycle. This limits the extent to which the Brayton cycle can be optimized. By redesigning the turbomachinery of the steam cycle, higher overall cycle efficiencies may be obtained. An entire combined cycle plant may be designed by upgrading the steam cycle's turbomachinery components to the newest technology.

A substantial quantity of heat is exhausted in the condenser of the steam cycle, and during Brayton cycle part load operation, high temperature helium is exhausted in addition to the condenser heat. The feasibility of utilizing this heat for useful purposes such as district heating or desalination can be examined.

The recuperated helium cycle resulted in a higher Brayton cycle efficiency but caused the temperature of helium entering the heat exchanger to fall below the acceptable level. Organic Rankine cycles operate at lower temperatures than steam cycles on account of the properties of the organic fluid. The use of an ORC as a bottoming cycle in place of a steam cycle could utilize the lower helium turbine exhaust temperature from a recuperated cycle.

The heat exchanger and helium bypass system can be analyzed in greater detail by implementing a more detailed model of the splitter and the mixer that is used during Rankine part load operation. Currently, a fixed pressure loss of 3 percent is assumed at the mixer. A more detailed analysis will provide better insight into the effect of the heat exchanger on the combined cycle efficiency.

Appendix A

NPSS Table for Off-Design Estimation of Helium Turbine and Helium Compressor Polytropic Efficiency

COMPRESSOR EFFICIENCY

```
real C_eff (real W)
	{
	Table eff (real m_frac)
		{
		m_frac = {
1,0.98,0.96,0.94,0.92,0.9,0.88,0.86,0.84,0.82,0.8,0.78,0.76,0.74,0.72,0.7}
			eff = {
0.905,0.904407346,0.903814692,0.899440342,0.893483838,0.886149479,0.87769671
8,0.868471011,0.858847435,0.849109572,0.839306627,0.829152195,0.818048572,0.8053409
37,0.79092621,0.776361854}

		interp = "linear";
		extrap = "none";
		}


	if( (switchDes == "OFFDESIGN") )
		{
		real m_frac = W/m_des_he; //m_des_he stores the design point value
of mass flow rate
		return(eff (m_frac));
		}
	else
		{
		return(0.905);
		}

	}
```

TURBINE EFFICIENCY

```
real T_eff (real W)
	{
	Table eff (real m_frac)
		{
		m_frac = {	1,	0.92,	0.9,	0.88,	0.86,	0.84,	0.82,
0.8,	0.78,	0.76,	0.74,	0.72,	0.7}
			eff = {	0.928,	0.925203864,	0.924296451,	0.922325598,
0.91931065,	0.915252054,	0.910131365,	0.903914727,	0.896559863,
0.888026552,	0.8782906,	0.867361314,	0.85530246}

		interp = "linear";
		extrap = "none";
		}


	if( (switchDes == "OFFDESIGN") )
```

```
        {
        real m_frac = W/m_des_he;
        return(eff (m_frac));
        }
else
        {
        return(0.928);
        }

}
```

References

[1] Merkel, T. C., Lin, H., Wei, X., and Baker, R., 2010, “Power Plant Post-Combustion Carbon Dioxide Capture: An Opportunity for Membranes,” Journal of Membrane Science, **359**(1-2), pp. 126–139.

[2] Desideri, U., and Paolucci, A., 1999, “Performance Modelling Of A Carbon Dioxide Removal System For Power Plants,” Energy Conversion and Management, **40**(18), pp. 1899–1915.

[3] Radosz, M., Hu, X., Krutkramelis, K., and Shen, Y., 2008, “Flue-Gas Carbon Capture on Carbonaceous Sorbents: Toward a Low-Cost Multifunctional Carbon Filter for ‘Green’ Energy Producers,” Industrial and Engineering Chemistry Research, **47**(10), pp. 3783–3794.

[4] Simpkin, W. E., 2014, “High efficiency power generation system and system upgrades,” Patent US20140338335 A1.

[5] Simões-Moreira, J. R., 2012, *Thermal Power Plant Performance Analysis*, Springer, London, pp. 7–39.

[6] Desai, N. B., and Bandyopadhyay, S., 2009, “Process Integration of Organic Rankine Cycle,” Energy, **34**(10), pp. 1674–1686.

[7] Schofield, J. R., 2010, "Design of a Heat Exchanger for Pebble Bed Reactor Applications," Project Report, Rensselaer Polytechnic Institute, Hartford, CT.

[8] Wang, C., 2003, “Design, Analysis and Optimization of the Power Conversion System for the Modular Pebble Bed Reactor System,” Ph.D. thesis, Massachusetts Institute of Technology, Cambridge, MA.

[9] Kadak, A. C., 2005, “A Future for Nuclear Energy: Pebble Bed Reactors,” International Journal of Critical Infrastructures, **1**(4), p. 330-345.

[10] Takizuka, T., Takada, S., Yan, X., Kosugiyama, S., Katanishi, S., and Kunitomi, K., 2004, “R&D on the Power Conversion System for Gas Turbine High Temperature Reactors,” Nuclear Engineering and Design, **233**, pp. 329–346.

[11] Rodriguez, S. B., Gauntt, R. O., Cole, R., Mcfadden, K., Gelbard, F., Drennen, T., Malczynski, L., Martin, B., Louie, D. L. Y., Archuleta, L., El-Genk, M., Tournier, J., Espinoza, F., Vierow, K., Hogan, K., Revankar, S. T., and Oh, S., 2007, "Development of Design and Simulation Model and Safety Study of Large-Scale Hydrogen Production Using Nuclear Power," SAND2007-6218, Albuquerque, NM.

[12] Simpkin HiEff Power, “High Efficiency (“Hi Eff”)Utility Rescue® Patent," (http://simpkin-hieff-power.com/)

[13] Apel, A., Byrd, R., Gardocki, M., 1996, "Numerical Propulsion System Simulation Architecture Definition," Computational Aerosciences Workshop, **13,** pp. 99–104.

[14] Lytle, J. K., 2000, “The Numerical Propulsion System Simulation: An Overview," NASA/TM-2000-209915, Glenn Research Center, Cleveland, OH.

[15] Vijaykumar, N., 2014, “Design and Multifidelity Analysis of Dual Mode Scramjet Compression System Using Coupled NPSS and Fluent Simulation,” M.S. thesis, The University of Texas at Arlington, Arlington, TX.

[16] Follen, G., auBuchon, M., 2000, “Numerical Zooming Between a NPSS Engine System Simulation and a One-Dimensional High Compressor Analysis Code,” NASA/TM-2000-209913, NASA, Cleveland, OH.

[17] Turner, M. G., Norris, A., Veres, J., 2004, "High Fidelity 3D Simulation of the GE90," AIAA-2003-3996, *33rd Fluid Dynamics Conference and Exhibit,* Orland, FL

[18] Claus, R. W., Lavelle, T., Townsend, S., Turner, M., 2008, "Coupled High-Fidelity Engine System Simulation," *26th ICAS*, pp. 1–10.

[19] “NPSS REFPROP Thermodynamic Property Package User Guide,” Wolverine Ventures, Florida, 2012.

[20] National Institute of Standards and Technology, "Thermophysical Properties of Fluid Systems," (http://webbook.nist.gov/chemistry/fluid/)

[21] "NPSS User Guide Reference Sheets," Wolverine Ventures, Florida, 2012.

[22] Tiwari, A. K., Islam, M., Khan, M. N., 2010, “Thermodynamic Analysis of Combined Cycle Plant,” International Journal of Engineering Science and Technology, **2**(4), pp. 480–491.

[23] Camporeale, S., and Fortunato, B., 1996, “Design and Off-Design Performance of Advanced Mixed Gas-Steam Cycle Power Plants,” IEEE, Washington, **2**, pp. 695–701.

[24] Dardour, S., Nisan, S., and Charbit, F., 2007, “Utilisation of Waste Heat from GT-MHR and PBMR Reactors for Nuclear Desalination,” Desalination, **205**, pp. 254–268.

[25] Castellano, R. N., 2012, *Alternative Energy Technologies : Opportunities and Markets*, Archives Contemporaines.

[26] Weber, P. T., 2011, "Modeling Gas Turbine Engine Performance at Part-Load," Electric Power Research Institute, Palo Alto, CA.

[27] U.S. Energy Information Administration, "How much carbon dioxide is produced per kilowatthour when generating electricity with fossil fuels?," (http://www.eia.gov/tools/faqs/faq.cfm?id=74&t=11)

Biographical Information

Warren Freitas was born on January 21st 1991. After developing an interest in aircrafts, he pursued and earned his Bachelor of Engineering degree in Aeronautical Engineering from Manipal University, India in 2013. During his senior year, he was a research intern at the Indian Institute of Science, Bengaluru, where his research focused on system identification of a UAV. His interest in aerodynamics and propulsion led him to pursue his Master of Science degree at the University of Texas, Arlington. Due to his interest in gas turbines and turbomachinery he joined the Aerodynamics Research Center and began his research on power plants. After graduating with his Master of Science degree, he plans to continue his research on turbomachinery and pursue his doctoral degree.